IEEE Access
Multidisciplinary | Rapid Review | Open Access Journal

IEEE SYSTEMS, MAN AND CYBERNETICS SOCIETY SECTION

Received 23 February 2024, accepted 19 March 2024, date of publication 22 March 2024, date of current version 28 March 2024.

Digital Object Identifier 10.1109/ACCESS.2024.3380918

APPLIED RESEARCH

Dynamic Smooth Sliding Control Applied to UAV Trajectory Tracking

ALESSANDRO JACOUD PEIXOTO, (Member, IEEE), WENDERSON G. SERRANTOLA, AND FERNANDO LIZARRALDE, (Senior Member, IEEE)

Department of Electrical Engineering, COPPE/UFRJ, Federal University of Rio de Janeiro, Rio de Janeiro 21941-617, Brazil

Corresponding author: Fernando Lizarralde (f.lizarralde@coppe.ufrj.br)

This work was supported in part by the Coordenação de Aperfeiçoamento de Pessoal de Nível Superior (CAPES), Brasil, under Finance Code 001; in part by CNPq/Brazil; and in part by FAPERJ.

ABSTRACT This paper proposes a sliding mode controller with a smooth control signal for a class of linear plants with nonlinear input state-dependent disturbance. The proposed controller is obtained by allowing some constant parameters of the earlier Smooth Sliding Control (SSC) to vary as a function of the output tracking error and its time derivative, improving the control chattering alleviation in practical implementations. Furthermore, during the sliding mode, the new scheme can synthesize a range of controllers, such as fixed gain PI controllers and approximations of the Super-Twisting Algorithm (STA). A complete closed-loop stability analysis is provided, leading to global stability properties, exact output regulation, and practical output tracking. In addition, realistic simulation results with an Unmanned Aerial Vehicle (UAV) model, incorporating aerodynamic effects and internal closed-loop controllers, are obtained and validated via experiments with a commercial hexacopter.

INDEX TERMS Chattering avoidance, sliding-mode control, super-twisting algorithm (STA), unmanned aerial vehicle (UAV), unmodelled dynamics.

I. INTRODUCTION

The number of UAV applications has been increasing in the last decade, mainly due to their maneuvering capability, allowing a variety of remote sensing and monitoring or inspection tasks [1], [2], [3]. In particular, the development of UAV trajectory tracking robust controls is crucial for the detection and identification of oil leaks in offshore environments, or for the extraction of traffic data via aerial video images [4], [5], [6], where the wind influence cannot be disregarded and an optimal desired trajectory in general is required to reduce the battery consumption, for instance.

Several control systems were proposed for the trajectory tracking problem of unmanned aerial vehicles. Classic techniques such as the Proportional-Integral-Derivative (PID) control have been applied to most existing flight control systems, because of their simple design and implementation, when is reasonable to approximate the vehicle dynamics to a linear model [7], [8], [9], with uniformly norm-bounded or almost constant disturbances. When the linearization process [10] is not valid, non-linear control methods come into play, such as optimization strategies for path planning [11], linear quadratic regulation control (LQR) [12], [13], feedback linearization control schemes [14], [15] and robust strategies via sliding modes [16], [17]. In addition, the performance of classic techniques is, in general, limited by the presence of uncertainties, disturbances, and unmodelled dynamics.

In contrast, it is well-known that sliding mode-based controllers are robust concerning external disturbances (eventually state/output dependent), parameter uncertainties, and unmodelled dynamics, but suffer from the chattering phenomenon. In this context, aiming to attenuate chattering, sliding mode control based on the Super-Twisting Algorithm has been widely applied [18], [19], [20], [21], [22], [23], [24]. Solutions for the trajectory tracking problem of UAVs have been pursued in the literature [25]. In [26] and [27], the altitude control of a quadrotor is based on a combined STA and high-order sliding mode (HOSM) observer, and in [28], a similar combination is addressed to estimate linear and angular velocities, and unknown lumped disturbance,

The associate editor coordinating the review of this manuscript and approving it for publication was Huiyan Zhang.

including experimental evaluation with the quadcopter DJI M100. To be able to cover inspection tasks with UAVs, manipulators have been attached, such as in [29], where an STA with gain adaptation law is designed in the presence of a disturbance caused by the manipulator dynamics.

Additionally, beyond affecting UAV's dynamics by adding manipulators, UAV geometric parameters can be variable over time [30] and the pick-and-place task can generate mass variation [31], [32]. In [30], a Fast Terminal Sliding Mode Controller was applied to guarantee the flight stability and rapid convergence of the states in finite time with a reconfigurable UAV. In [31], a sliding mode technique was proposed allowing the UAV control to adapt to the altered mass without re-tuning the controller and, in [32], the landing problem on a moving platform was solved together with a pick-and-place task, by using the so-called SSC scheme.

The SSC was presented in [33], as an alternative modification in the Variable Structure Model Reference Control (VS-MRAC) [34], [35], to provide a smooth control effort, since the VS-MRAC is a strategy with discontinuous control effort. It introduces an averaging filter to obtain a continuous control signal. To compensate for the phase lag added by the averaging filter, an internal prediction loop was employed so that the ideal sliding mode could be preserved, leading to chattering avoidance and robustness concerning unmodelled dynamics [36]. Recently, this strategy was generalized for plants with time-varying control gain and applied to the autonomous landing problem in a moving platform [32]. More recently, in [37] was presented a new SSC scheme with the averaging filter time constant being updated via the tracking error for a real UAV trajectory tracking application.

In this paper, a novel extension of the results of [37] is proposed. As the main contributions of the paper, we consider: (i) the development of the new (dynamic) SSC scheme, named Dynamic Smooth Sliding Control (DSSC), where the original fixed parameters of the SSC averaging filter and the predictor are replaced by functions that are updated via the tracking error; (ii) a complete closed-loop stability analysis of the DSSC algorithm for the considered class of linear plants with nonlinear disturbance; (iii) a connection of the synthesized DSSC during sliding mode with the Variable Gain Super-Twisting Algorithm (VGSTA) and the standard STA, by selecting appropriate functions in the DSSC; and (iv) experimental evaluation of the DSSC for trajectory tracking in a real-world scenario with the commercial DJI M600 Pro hexacopter.

A. NOTATIONS AND TERMINOLOGIES

A mixed time-domain and frequency-domain notation will be adopted to avoid clutter. In this manner, a rational function $G(s)$ will denote either an operator, where s is the differential operator, or a transfer function, where s is the Laplace complex frequency variable. Therefore, the time and frequency dependencies of the signals will be mostly omitted. In general, for a scalar composite function $f(e(t), \sigma(t), t)$, where $e(t)$ and $\sigma(t)$ are scalar functions of the time instant $t \geq 0$ (time-varying functions), we perform along the paper the abuse of notation $f(t) = f(e(t), \sigma(t), t)$.

B. MOTIVATION FOR THE CONSIDERED CLASS OF PLANTS

In this paper, the trajectory tracking control problem of a UAV is addressed. The proposed control scheme considers that an internal Kalman filter provides full state estimation, and **inaccessible** inner controllers are responsible for decoupling the four UAV degrees of freedom, corresponding to the UAV's linear velocity and to the yaw angle rate, see Figure 1, allowing to perform a cascade control strategy. The UAV dynamic model is given by:

$$\begin{aligned} \mathcal{M}\dot{v} &= -\mathcal{M}ge_3 + Rfe_3 + F_{drag}\,, \\ \mathcal{J}\dot{\Omega} &= -(\Omega \times \mathcal{J}\Omega) + M + \tau_{drag} + \tau_{dist}\,, \\ \dot{R} &= R \times \Omega\,, \\ \dot{\psi} &= e_3^T J_R^{-1} \Omega\,, \end{aligned} \tag{1}$$

where $\Omega \in \mathbb{R}^3$ is the angular velocity represented in the body frame, $v = \begin{bmatrix} v_x & v_y & v_z \end{bmatrix}^T \in \mathbb{R}^3$ is the UAV's linear velocity vector (in the inertial frame), R represents the rotation matrix from the body frame to the inertial frame, J_R is the Jacobian Euler angles representation, $v_\psi = \dot{\psi}$ is the yaw angle velocity, g is the gravity acceleration, $\mathcal{J}$ is the (diagonal) inertia matrix, $\mathcal{M} \in \mathbb{R}$ is the UAV mass, $e_3 = \begin{bmatrix} 0 & 0 & 1 \end{bmatrix}^T$, $M \in \mathbb{R}^3$ is the *net moment* and $f = \sum_{i=1}^{n_r} f_i$ is the *net thrust magnitude*, where $f_i \in \mathbb{R}$ is the i-th propeller's thrust magnitude and n_r is the number of rotors. The drag terms are incorporated in F_{drag} and τ_{drag} and τ_{dist} is a torque disturbance depending on the propellers' angular velocity and acceleration, see details in the Appendix A. The inner controllers generate the torques and forces commands via propellers' thrusts for tracking the velocity references (u_x, u_y, u_z or u_ψ) generated by the outer controller (DSSC), which in turn is designed for tracking position and orientation, i.e., to assure that the UAV position p_x, p_y, p_z track the desired positions $p_{x_d}, p_{y_d}, p_{z_d}$ and that the yaw angle ψ tracks the desired angle ψ_d. For the dynamics of each degree of freedom (DOF), the inner controllers and the Kalman filter can be treated as unmodelled dynamics for the outer controller (DSSC), so that a kinematic model from velocities commands to actual velocities is considered.

We consider the complete model for the UAV based on the following premises and motivations:

1) Low/medium velocity profiles are considered so that the motors and the motors drivers (ESCs) dynamic can be neglected, as well as, the internal Kalman Filter dynamics of the UAV leading to the availability of the full UAV state vector.
2) The proposed DSSC scheme acts as an outer controller that provides velocity commands as references for the inner velocity control loops. These inner velocity control loops are designed so that a reasonable control performance is achieved.[1]

[1]However, the outer controller can compensate for the eventual low performances of the inner controllers.

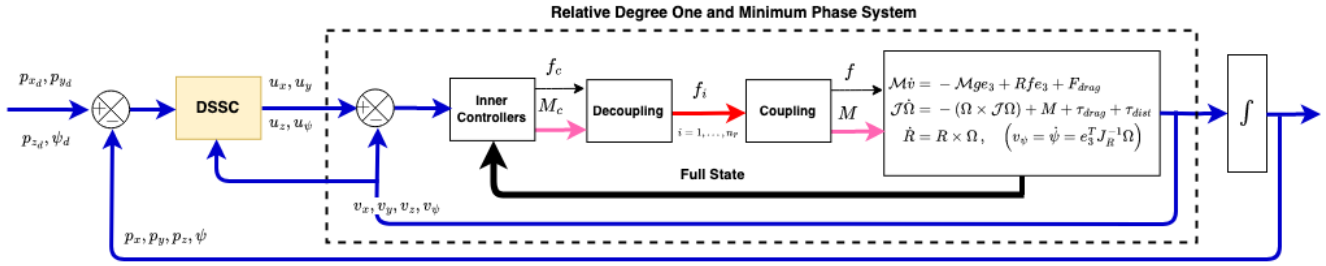

FIGURE 1. The inner and outer control topology for UAV trajectory tracking. The inner controllers are PI controller with feedback linearization and feedforward terms. The DSSC outer controller is provided in Table 1. Ideally, the decoupling/coupling blocks are constant matrices depending only on the UAV geometry such that $M = M_c$ and $f = f_c$.

As a motivation for the class of plants considered in this paper, let us describe shortly the resulting closed-loop dynamics with a given inner controller for the altitude degree of freedom. The same idea can be extended to the other degrees of freedom.

Here, the control objective is to assure that the altitude velocity v tracks the desired velocity command u, at least, with some residual error. From the last component of the v-dynamics $\mathcal{M}\dot{v} = -\mathcal{M}ge_3 + Rfe_3 + F_{drag}$, see Figure 1, one possible control law is given by a composition of a feedback linearization control term $f := \mathcal{M}(\mathcal{U} + g)$, which is parameter dependent, and a PI-control law $\mathcal{U} := -k_p(v - u) - k_i \int_0^t (v(\tau) - u(\tau))d\tau$, where the roll and pitch angles are considered small. The closed-loop dynamic behavior from the velocity command input u to the actual velocity v is given by

$$(\ddot{v} - \ddot{u}) = -k_p(\dot{v} - \dot{u}) - k_i(v - u) + \left[\dot{\mathcal{D}} - \ddot{u}\right], \quad (2)$$

where $\mathcal{D} = e_3^T F_{drag}/\mathcal{M}$ is a disturbance due to the aerodynamic drag F_{drag}, see Figure 1. Thus, by choosing the control gains appropriately one can impose an acceptable closed-loop performance and conclude that, for low acceleration commands ($\ddot{u} \approx 0$) and for low aerodynamic drag, $e(t) := v - u$ tends to zero, as $t \to \infty$. For any eventual residual error in the inner control loop, the outer position control loop (DSSC) can compensate for it. Moreover, a more elaborate inner controller could be considered [38], but this is not the focus of this paper.

The closed-loop system (2) can be represented by $v = G(s)(u + d)$, where $G(s) = \frac{(k_p s + k_i)}{(s^2 + k_p s + k_i)}$ and $d = \frac{s}{(k_p s + k_i)}\mathcal{D}$. Note that $G(s)$ is a **relative degree one and minimum phase** ($k_p, k_i > 0$) transfer function from $u + d$ to v. This system can be written in state-space in the normal form as

$$\dot{\eta} = a_\eta \eta + b_\eta v\,, \quad (3)$$
$$\dot{v} = -a_p v - c_\eta \eta + k_p(u + d)\,, \quad (4)$$

where $\eta \in \mathbb{R}$ is the zero dynamics state vector (for details, see Appendix B). The disturbance d could also incorporate other eventually remaining terms due to any mismatch parameters in the feedback linearization control term.

In what follows, motivated by (3)–(4), a class of relative degree one and minimum phase plants, of arbitrary order, is considered for the linear position and yaw angle tracking control problem formulation.

II. PROBLEM FORMULATION: ONE DEGREE OF FREEDOM

Consider the following class of uncertain plants given by

$$\dot{\eta}(t) = A_\eta \eta(t) + B_\eta x_2(t)\,, \quad (5)$$
$$\dot{x}_1(t) = x_2(t)\,, \quad (6)$$
$$\dot{x}_2(t) = -a_p x_2(t) - C_\eta \eta + k_p[u_p(t) + d(y, \dot{y}, t)]\,, \quad (7)$$
$$y(t) = x_1(t)\,, \quad (8)$$

where $u_p \in \mathbb{R}$ is the control input, $y \in \mathbb{R}$ is the plant output, $\eta \in \mathbb{R}^{n-2}$ is the *inverse system* (zero dynamics) state vector, $d \in \mathbb{R}$ is regarded as a matched input disturbance, $k_p > 0$ is the uncertain high-frequency gain (HFG), a_p is an uncertain parameter, and

$$x := \begin{bmatrix} x_1 & x_2 \end{bmatrix}^T := \begin{bmatrix} y & \dot{y} \end{bmatrix}^T \in \mathbb{R}^2$$

is the state vector. Without loss of generality, consider that the inverse system has a state-space realization (A_η, B_η, C_η), with (A_η, B_η) in the canonical controllable form with $B_\eta = \begin{bmatrix} 0 \ldots 0 & 1 \end{bmatrix}^T \in \mathbb{R}^{n-2}$. We assume that A_η is a Hurwitz matrix (minimum phase assumption) and η **is unavailable for feedback**. The uncertain function $d(y, \dot{y}, t)$ is assumed piecewise continuous in t and locally Lipschitz continuous in the other arguments. For each solution of (5)–(7), there exists a maximal time interval of definition given by $[0, t_M)$, where t_M may be finite or infinite. Thus, finite-time escape is not precluded *a priori*. Regarding the application covered in this paper, in (7)–(8), y is a generic output representing a UAV's degree of freedom (p_x, p_y, p_z or ψ) and u_p is the corresponding generic velocity command input (u_x, u_y, u_z or u_ψ), see Figure 1.

Remark 1 Plant Input Disturbance: UAV's Application: In (5)–(8), the input disturbance $d(y, \dot{y}, t)$ represents the coupling between degrees of freedom, the wind influence, and possible nonlinearities remaining due to some unmatched parameters in the inner velocity loop. Moreover, it is considered that the wind velocity has low-frequency components or can be represented by piecewise functions with jump discontinuities where the discontinuity points have zero measure. ■

A. CONTROL OBJECTIVE

The aim is to achieve global convergence properties in the sense of uniform signal boundedness and asymptotic output practical tracking. The control objective is to design a control law $u_p(t)$ for the uncertain plant (5)–(8) such that $y(t)$ tracks a bounded desired trajectory $y_m(t)$ as close as possible, i.e., the tracking error

$$e(t) := y(t) - y_m(t)\,, \tag{9}$$

converges to zero as $t \to +\infty$, or at least, to the neighborhood of zero (practical tracking). The *desired trajectory* $y_m(t)$ is assumed to be smooth enough so that $\dot{y}_m$ and $\ddot{y}_m$ are well defined *available* signals.

For the sake of simplicity and to focus on the novelty of the proposed controller (DSSC) in comparison to the previous version (SSC), we assume that y and $\dot{y}$ are available for feedback. Furthermore, as mentioned before, the application considered in the paper endorses this assumption.

Let the *relative degree one output variable* $\sigma(y, \dot{y}, t) : \mathbb{R}^3 \to \mathbb{R}$ be defined by

$$\sigma := \dot{e} + l_0 e\,. \tag{10}$$

The main idea is to design u_p so that σ tends to zero as $t \to +\infty$, or at least, to the vicinity of zero, despite the input disturbance $d(y, \dot{y}, t)$. Thus, the convergence of the tracking error $e(t)$ to a residual set is assured by setting $l_0 > 0$, according to (10).

The extension to the case where only y is available for feedback can be obtained by using the approximation $\dot{y} \approx y_f := \frac{s}{(\tau_f s+1)} y$, with $\tau_f > 0$ being a design constant, and extension to systems with an arbitrary relative degree can be obtained by using a linear lead filter, a high gain observer (HGO) [39], or a robust exactly differentiator (RED) [40], as in [36], [41], and [42].

B. ERROR DYNAMICS

Let the control signal be composed of two terms

$$u_p(t) = u(t) + u^n(t)\,, \tag{11}$$

where the control effort u is the DSSC robust control effort and u^n is a *nominal control law*, both to be defined later on.

In practical applications there exists some level of knowledge of the plant parameters and, in general, a nominal control based on this knowledge can be applied to reduce the magnitude of the robust action (here being the DSSC), which is designed to deal with disturbances and/or parameter uncertainties.

From (10), the e-dynamics is directly obtained as

$$\dot{e} = -l_0 e + \sigma\,. \tag{12}$$

Moreover, from (10), one has $\dot{\sigma} = \ddot{y} + l_0\dot{y} - \dot{\sigma}_m$, where $\sigma_m := \dot{y}_m + l_0 y_m$. Moreover, from (6)–(7) and (11) one can write $\ddot{y} = -a_p\dot{y} + k_p(u + u^n) + k_p(d - C_\eta\eta/k_p)$. Therefore, the σ-dynamics is given by

$$\dot{\sigma} = k_p u + d_\sigma\,, \tag{13}$$

where $d_\sigma := k_p u^n + (l_0 - a_p)\dot{y} - \dot{\sigma}_m + k_p d - C_\eta\eta$ is treated as a disturbance term.

III. DYNAMIC SMOOTH SLIDING CONTROL (DSSC)

In Figure 2, it is illustrated the DSSC block diagram, which has the same structure as the original SSC [33], [43], [44]. In comparison to the SSC, the **Dynamic SSC** (DSSC) differs in one main aspect: the averaging filter time constant τ_{av}, the predictor time constant τ_m and the predictor gain k_o are allowed to vary with the time t and/or the plant signals $\sigma(t)$ and $e(t)$. The DSSC law is given by

$$u := -u_0^{av}\,, \tag{14}$$

with a time-varying averaging filter

$$\tau_{av}(t)\,\dot{u}_0^{av} = -u_0^{av} + u_0\,, \tag{15}$$

where $\tau_{av}(t) = \tau_{av}(\sigma(t), e(t), t) > 0$ $(\forall \sigma, e, t)$ and

$$u_0 = \varrho(t)\,\mathrm{sgn}(\tilde{\sigma})\,, \quad \varrho(t) > 0\,, \tag{16}$$

is the predictor's discontinuous term, with modulation function $\varrho(t)$. In the DSSC, *the sliding variable* $\tilde{\sigma}$ is defined as

$$\tilde{\sigma} := \sigma - \hat{\sigma}\,, \tag{17}$$

where $\hat{\sigma}$ is the output of the predictor

$$\dot{\hat{\sigma}} = -\frac{1}{\tau_m(t)}\hat{\sigma} + k_o(t)[-u_0^{av} + u_0]\,, \tag{18}$$

with $\tau_m(t) = \tau_m(\sigma(t), e(t), t) > 0$ $(\forall \sigma, e, t)$ and $k_o(t) = k_o(\sigma(t), e(t), t) > 0$ $(\forall \sigma, e, t)$. Note that, all the functions

$$k_o(t)\,,\, \tau_m(t)\,,\, \tau_{av}(t)\,,\, \varrho(t)\,,$$

can depend on exogenous time-varying functions, as well as, on the output tracking error e (or σ), which in turn depends on the closed-loop system dynamics. Henceforth, we denote these functions by **state-dependent functions**. The DSSC's block diagram is presented in Figure 2, including the linear lead filter for completeness of the presentation.[2]

A. EXISTENCE OF IDEAL SLIDING MODE

With $\tilde{\sigma}$ defined in (17), the σ-dynamics in (13) and the smooth control law (14), one has that $\dot{\tilde{\sigma}} = \dot{\sigma} - \dot{\hat{\sigma}} = [-k_p u_0^{av} + k_p u^n + (l_0 - a_p)\dot{y} + k_p(d - C_\eta\eta/k_p) - \dot{\sigma}_m] - \dot{\hat{\sigma}}$. Moreover, by using the predictor dynamics in (18) and the relationship $\hat{\sigma} = \sigma - \tilde{\sigma}$, one can further obtain

$$\tau_m\dot{\tilde{\sigma}} = -\tilde{\sigma} + k_o\tau_m[-u_0 + d_0/k_o]\,, \tag{19}$$

where

$$d_0 := (k_o - k_p)u_0^{av} + \tilde{d}_1 + \tilde{d}_2\,, \tag{20}$$

[2]Despite that, the original SSC [33] can be applied for a broader class of plants with arbitrary relative degree [43] and [44], we focus on the case where y and $\dot{y}$ are available for feedback. However, the DSSC scheme can also deal with arbitrary relative degree plants, by using linear lead filters to estimate output time derivatives. We restrict ourselves to the case of relative degree one which is the simplest case amenable by pure Lyapunov design.

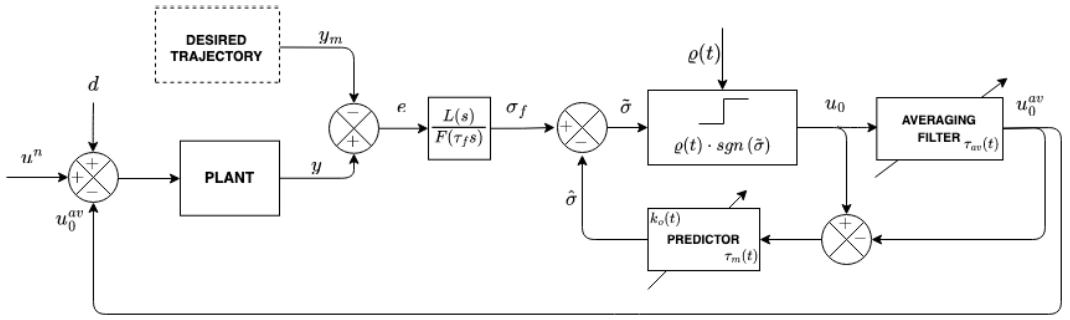

FIGURE 2. General DSSC block diagram for arbitrary relative degree case and with generic state-dependent functions $\tau_m(\sigma(t), e(t), t)$, $k_o(\sigma(t), e(t), t)$ and $\tau_{av}(\sigma(t), e(t), t)$. The predictor is given in (18) and depends on k_o and τ_m, while the averaging filter is given in (15) and depends on τ_{av}. For the class relative degree one plants considered here with $\dot{y}$ available for feedback, one can set $\tau_f = 0$, so that $\sigma_f = \sigma$ with σ in (10).

with $\tilde{d}_1 := k_p u^n - a_p \dot{y} + k_p(d - C_\eta \eta / k_p)$ being an uncertain term and $\tilde{d}_2 := \sigma/\tau_m + l_0 \dot{y} - \dot{\sigma}_m$ being a known signal that could be directly canceled by redefining the control term u_0 in (16). For simplicity, at the cost of being more conservatism, we treat $\tilde{d}_2$ as an uncertain term too.

As in the original SSC, sliding mode occurs at $\tilde{\sigma} \equiv 0$ so that $\tilde{\sigma}$ converges to zero in some finite time $t_s \in [0, t_M)$, i.e., $\hat{\sigma}(t) = \sigma(t), \forall t \in [t_s, t_M)$, provided that the modulation function ϱ (in the discontinuous term u_0) satisfies

$$\varrho > d_0/k_o \,,$$

modulo vanishing terms due to initial conditions, i.e., being designed to dominate the norm of the total disturbance d_0/k_o faced by u_0 in the (19), after some initial transient. The proof of the sliding mode existence and the avoidance of finite time escape (mainly due to the unboundedness observability property of the closed-loop system) are provided later on in Theorem 1.

B. MAIN FEATURES OF THE PROPOSE DSSC

The main features of the new DSSC scheme can be summarized as follows: (i) the algorithm presents robustness w.r.t. unmodelled dynamics and global/semi-global stability properties (the full proof is provided), and (ii) it is observed an improvement w.r.t. the previous SSC, where a better control chattering alleviation is obtained.

The complete closed-loop stability analysis is one of the main contributions of this paper and it is provided later on for the class of plants (5)–(8). In addition, the robustness of the proposed control scheme (DSSC) w.r.t. unmodelled dynamics is verified in the experiments with the DJI M600 and via numerical simulations with the full coupled dynamics model, including the inner controllers and aerodynamic effects, corroborating that a relative degree one is fair enough for representing each of the four DOF, mainly for low/medium velocity profiles. Any residual coupling between the DOFs is embedded in an input disturbance.

Moreover, with this modification in the original SSC, one can observe an improvement in control chattering alleviation in practical implementations where discretization, for instance, generates numerical chattering even for the relative degree one case. Let us explain this improvement when the averaging filter has a pass-band inversely proportional to $|e(t)|$. First, we point out that in both the SSC and the DSSC, sliding mode occurs in an internal variable different from the output tracking error e. In general, sliding mode takes place from the beginning, when $|e|$ can be large, as well as, the modulation function ϱ. Second, in the SSC, practical tracking is obtained in the sense that the tracking error converges to a residual set $\mathcal{O}(\tau_{av})$ proportional to the **fixed** averaging filter time constant τ_{av}. In the DSSC, in contrast, the residual set is proportional to the steady-state value τ_{av}^* of $\tau_{av}(e(t))$.

Thus, to obtain high tracking precision in the SSC, the fixed time constant should be small, while in the DSSC, only the steady-state value τ_{av}^* should be small. It means that, if one set $\tau_{av}(e(t)) \propto |e(t)| + \mathcal{O}(\tau_{av}^*)$, then the DSSC filters out the high frequencies of the switching control more than the SSC, exactly in the time interval where the modulation function and the tracking error are large. When e is small, the filter can allow high frequencies to pass, since the modulation function is small. The final result is a smoother control action when compared with the original SSC, maintaining at least the same level of tracking precision.

IV. DESIGN OF THE STATE-DEPENDENT FUNCTIONS OF THE DSSC

As mentioned in Section III-A, the modulation function ϱ is designed to overcome the disturbance in the $\tilde{\sigma}$-dynamics (19) to assure ideal sliding mode at the manifold $\tilde{\sigma} = 0$. After achieving the ideal sliding mode, an equivalent synthesized controller results. This synthesized controller depends on the state-dependent functions τ_{av}, τ_m and k_o. At this point, we have freedom to choose the DSSC functions.

A. GENERAL SYNTHESIZED EQUIVALENT CONTROLLER DURING SLIDING MODE

Now, let us find a general formulation for the synthesized equivalent DSSC control law during sliding mode. First, denote $\bar{u}_0^{av} = u_0^{av}$ as the solution of (15), when the discontinuous control u_0 is replaced by the *equivalent control*

$u_{eq} = \frac{d_0}{k_o}$, directly obtained from the $\tilde{\sigma}$-dynamics (19). This is the so called *reduced dynamics* $\tau_{av}(t)\dot{\bar{u}}_0^{av} = -\bar{u}_0^{av} + u_{eq}$. Also replace u_0 by u_{eq} in the predictor dynamics (18), leading to $\tau_m(t)\dot{\hat{\sigma}} = -\hat{\sigma} + \tau_m(t)k_o(t)[\tau_{av}(t)\dot{\bar{u}}_0^{av}]$. Since, during sliding mode at $\tilde{\sigma} = 0$ one has $\hat{\sigma} = \sigma$, then one can further write

$$\tau_m(t)\dot{\sigma} = -\sigma + \tau_m(t)k_o(t)[\tau_{av}(t)\dot{\bar{u}}_0^{av}], \tag{21}$$

leading to the time derivative of the synthesized DSSC law $\bar{u} := \bar{u}_0^{av}$ given by[3]

$$\dot{\bar{u}}(t) = -\left[\frac{1}{k_o(t)\tau_{av}(t)}\right]\dot{\sigma}(t) - \left[\frac{\sigma(t)}{k_o(t)\tau_{av}(t)\tau_m(t)}\right]. \tag{22}$$

Let us rewrite the terms in square brackets of (22) in a more convenient form for selecting the DSSC functions $k_o(t)$, $\tau_{av}(t)$ and $\tau_m(t)$, in terms of σ, e and t. One can find appropriate functions $g_1(t) = g_1(\sigma(t), e(t), t)$ and $g_2(t) = g_2(\sigma(t), e(t), t)$ such that

$$\left[\frac{1}{k_o\tau_{av}}\right] = \frac{\partial[g_1\sigma]}{\partial\sigma}, \quad \text{and}$$
$$\left[\frac{\sigma}{k_o\tau_{av}\tau_m}\right] = \left[\frac{\partial(g_1\sigma)}{\partial e}\dot{e} + \frac{\partial(g_1\sigma)}{\partial t} + g_2\sigma\right]. \tag{23}$$

The functions $g_1(\sigma, e, t) > 0$ and $g_2(\sigma, e, t) > 0$ must be chosen sufficiently smooth and so that $k_o, \tau_{av} > 0$ and $\tau_m > 0$ are well-defined for all finite values of σ, e and t. Then, (22) can be rewritten as

$$\dot{\bar{u}}(t) = -\frac{d\,[g_1(t)\sigma(t)]}{dt} - g_2(t)\sigma(t). \tag{24}$$

Therefore, by integrating both sides of (24), the synthesized DSSC law can be written as:

$$\bar{u}(t) = -g_1(t)\sigma(t) - \int_{t_s}^{t} g_2(\tau)\sigma(\tau)d\tau + C_s, \tag{25}$$

$\forall t \geq t_s$, where $C_s := \bar{u}(t_s) + g_1(t_s)\sigma(t_s)$ is a constant[4] and $g_1(t)$ and $g_2(t)$ are nonlinear gains that should be designed so that the functions $k_o(t)$, $\tau_m(t)$ and $\tau_{av}(t)$ be positive.

Depending on the choices for the nonlinear gains g_1 and g_2 the resulting synthesized controller has different structures and properties. In fact, as illustrated in Appendix C, one can arrive at synthesized controllers starting from a simple PI controller, passing through an approximation for the standard STA [16], [18], to approximation for the variable gain STA (VGSTA) [19], [23].

A simple PI control or the standard STA (with constant gains) can deal with second-order plants, without inverse dynamics. However, as in [19] and [23], plants with inverse dynamics require the STA's gains to be state-dependent, leading to the VGSTA.

Our focus is on the choice for g_1 and g_2 which leads to an approximation for the VGSTA since the plant (5)–(7) has inverse dynamics, which is considered in the complete stability analysis given later on in Theorem 1.

[3]The DSSC can also be designed for high-order plants with arbitrary relative degrees, in this case, the synthesized controller has more terms than (22).

[4]This constant is an unknown constant. However, this is not an issue since the expression for $\bar{u}$ is used only for analysis purposes.

B. A PARTICULAR SYNTHESIZED CONTROLLER

Let $\hat{\phi}_2(\sigma) := \hat{\phi}_1(\sigma)\hat{\phi}_1'(\sigma)$ with $\hat{\phi}_1$ defined as

$$\hat{\phi}_1(\sigma) := \frac{\phi_a\sigma}{(|\sigma|^{1/2} + \delta)} + \phi_b\sigma, \tag{26}$$

where $\hat{\phi}_1(\sigma)$ can be rewritten as

$$\hat{\phi}_1(\sigma) = \left[\frac{\phi_a|\sigma|^{1/2}}{(|\sigma|^{1/2} + \delta)}\right]|\sigma|^{1/2}\text{sgn}(\sigma) + \phi_b\sigma,$$

$\delta > 0$ is an arbitrary small constant and $\phi_a > 0$ and $\phi_b > 0$ are design constants. Note that

$$\hat{\phi}_1' = \phi_a\left[\frac{(|\sigma|^{1/2} + 2\delta)}{2(|\sigma|^{1/2} + \delta)^2}\right] + \phi_b.$$

By **defining** the nonlinear variable gains g_1 and g_2 as

$$g_1\sigma = \kappa_1\hat{\phi}_1, \quad \text{and} \quad g_2\sigma = \kappa_2\hat{\phi}_2 = \kappa_2\hat{\phi}_1\hat{\phi}_1', \quad \sigma \neq 0,$$

and $g_1 = g_2 = 0$, for $\sigma = 0$, the synthesized DSSC law (25) becomes $\bar{u} = \hat{u}_{vgsta} + C_s$, with $C_s := \bar{u}(t_s) + \kappa_1(t_s)\hat{\phi}_1(t_s)$ and

$$\hat{u}_{vgsta}(t) = -\kappa_1(t)\hat{\phi}_1(t) - \int_{t_s}^{t}\kappa_2(\tau)\hat{\phi}_2(\tau)d\tau. \tag{27}$$

For $\phi_a = 1$ and $\phi_b = \kappa_3$, the control law (27) is an approximation for the VGSTA control law $u_{vgsta}(t) := -\kappa_1\phi_1(\sigma(t)) - \int_{t_s}^{t}\kappa_2\phi_2(\sigma(\tau))d\tau$, of [19] and [23], with $\phi_1(\sigma) := |\sigma|^{1/2}\text{sgn}(\sigma) + \kappa_3\sigma$ and $\phi_2(\sigma) := \phi_1'(\sigma)\phi_1(\sigma)$.

Now, since the variable gains $\kappa_1 > 0$ and $\kappa_2 > 0$ are functions of the time t and the plant's states σ and e, then from (23), one has to select the DSSC's state-dependent functions k_o, τ_{av} and τ_m to satisfy

$$\left[\frac{1}{k_o\tau_{av}}\right] = \left[\kappa_1'\hat{\phi}_1 + \kappa_1\hat{\phi}_1'\right],$$

and

$$\left[\frac{\sigma}{k_o\tau_{av}\tau_m}\right] = \hat{\phi}_1\left[\frac{\partial\kappa_1}{\partial e}\dot{e} + \frac{\partial\kappa_1}{\partial t} + \kappa_2\hat{\phi}_1'\right].$$

Thus, one has to select k_o, τ_{av} and τ_m so that

$$k_o\tau_{av} := \frac{1}{\left[\kappa_1'\hat{\phi}_1 + \kappa_1\hat{\phi}_1'\right]}, \tag{28}$$

and

$$\tau_m := \frac{\left[\kappa_1'\hat{\phi}_1 + \kappa_1\hat{\phi}_1'\right]}{\left[\frac{\phi_a}{(|\sigma|^{1/2}+\delta)} + \phi_b\right]\left[\frac{\partial\kappa_1}{\partial e}[-l_0e + \sigma] + \frac{\partial\kappa_1}{\partial t} + \kappa_2\hat{\phi}_1'\right]}, \tag{29}$$

where the relationship $\dot{e} = -l_0e + \sigma$ was used. Note that, in (28), an extra degree of freedom is allowed for choosing k_o and τ_{av}: (i) k_o being a constant function and τ_{av} time-varying function or vice-versa and (ii) both being time-varying functions.

In fact, the variable gains $\kappa_1(\sigma, e, t) > 0$ and $\kappa_2(\sigma, e, t) > 0$ must be designed so that $\tau_{av} > 0$ and $\tau_m > 0$ are well-defined for all finite values of σ, e. The DSSC's

state-dependent functions and the design guidelines of the corresponding control parameters are given in Appendix F and summarized in Table 1.

The synthesized equivalent controller approaches the VGSTA, far from the origin of the state-space (σ, e), and acting like a reduced gain version of the VGSTA, near the origin.

V. THE CASE STUDIED: STABILITY RESULTS, NUMERICAL SIMULATIONS, AND EXPERIMENTAL RESULTS

In what follows, we provide the main stability results with the DSSC functions in Table 1, the corresponding numerical simulations with the full UAV's dynamic model (1), including the aerodynamic effects and the inner control loops, and with the model (5)–(8), and the corresponding experimental results obtained with the commercial DJI M600 Pro hexacopter.

A. CLOSED-LOOP STABILITY RESULTS

To obtain the stability result and perform the full stability analysis, some assumptions must be considered. The plant parameters k_p and a_p in (7) are assumed uncertain with known bounds and we consider a class of input disturbances that can be partitioned as

$$d(y, \dot{y}, t) := d_1(y, \dot{y}, t) + d_2(y, t) + d_3(t)\,. \tag{30}$$

The following assumption is considered:

(A0.a) There exist positive constants $\underline{k}_p$, $\bar{k}_p$ and $\bar{a}_p$, such that

$$0 < \underline{k}_p \leq |k_p| \leq \bar{k}_p \quad \text{and} \quad |a_p| \leq \bar{a}_p\,,$$

where $\underline{k}_p$ and $\bar{a}_p$ are known constants.

(A0.b) There exists a known non-negative scalar function $\alpha_d(y, \dot{y}, t) : \mathbb{R}^3 \to \mathbb{R}^+$, locally Lipschitz in y and $\dot{y}$, piecewise continuous and upper bounded in t such that the input disturbance $d(y, \dot{y}, t)$ satisfies

$$|d(y, \dot{y}, t)| \leq \alpha_d(y, \dot{y}, t)\,, \quad \forall y, \dot{y}\,, \quad \forall t \in [0, t_M)\,,$$

with $\alpha_d(y, \dot{y}, t) < \alpha_\sigma(|\sigma|) + \alpha_e(|e|) + \alpha_t(t)$, where α_σ, α_e are class-$\mathcal{K}$ functions and α_t is a non-negative scalar function upper bounded in t.

Regarding the input disturbance partition (30), we also assume that:

(A1) There exist known constants $k_{d1} \geq 0$, $k_{d2} \geq 0$ and $k_{d3} \geq 0$ and known a non-negative scalar function $\alpha_{d1}(y, \dot{y}, t) : \mathbb{R}^3 \to \mathbb{R}^+$, locally Lipschitz in y and $\dot{y}$, piecewise continuous and upper bounded in t such that the term $d_1(y, \dot{y}, t)$ in (30) satisfy

$$|d_1(y, \dot{y}, t)| \leq \alpha_{d1}(y, \dot{y}, t)|\sigma|\,, \quad \forall y, \dot{y}\,,$$

and $\forall t \in [0, t_M)$, with $\alpha_{d1}(y, \dot{y}, t) := k_{d1}|y| + k_{d2}|\dot{y}| + k_{d3}$ and $\sigma(y, \dot{y}, t)$ in (10).

(A2) There exist known constants $k_{d4} \geq 0$ and $k_{d5} \geq 0$ and a known non-negative scalar function $\alpha_{d2}(t) : \mathbb{R} \to \mathbb{R}^+$, piecewise continuous and upper bounded in t, such that the term $d_2(y, t)$ in (30) satisfies $\left|\frac{\partial d_2(y,t)}{\partial y}\right| \leq k_{d4}$ and $\left|\frac{\partial d_2(y,t)}{\partial t}\right| \leq k_{d5}|y| + \alpha_{d2}(t)$, $\forall t \in [0, t_M)$.

(A3) There exists a known non-negative scalar function $\alpha_{d3}(t) : \mathbb{R} \to \mathbb{R}^+$, piecewise continuous and upper bounded in t, such that the time derivative of the term $d_3(t)$ in (30) satisfies $|\dot{d}_3(t)| \leq \alpha_{d3}(t)$, $\forall t \in [0, t_M)$.

Before state the main theorem, let us define the *nominal control law* composed by: (i) a feedforward term $u_m^n(t)$; (ii) $u_p^n(e(t))$, representing a proportional feedback action; (iii) $u_d^n(\sigma(t))$, contributing to a derivative plus proportional feedback action (since $\sigma = l_0 e + \dot{e}$); and (iv) $u_i^n(t) = \int_0^t \bar{u}_i^n(e(\tau), \sigma(\tau))d\tau$, as an integral feedback action. The nominal control is written in the form

$$u^n(t) := u_p^n(t) + u_d^n(t) + u_i^n(t) + u_m^n(t)\,, \tag{31}$$

where $u_p^n(t) = u_p^n(e(t))$ and $u_d^n(t) = u_d^n(\sigma(t))$. For simplicity and without loss of generality, we restrict the nominal control to have terms that satisfy the following additional assumption:

(A4) There exist non-negative constants c_σ, c_{e1}, c_{e2}, $c_{i\sigma}$, c_{ie} and c_m such that

$$\begin{aligned} |u_p^n(e)| &\leq c_{e1}|e|\,, \quad \left|\frac{du_p^n(e)}{de}\right| \leq c_{e2}\,, \\ |\bar{u}_i^n(e, \sigma)| &\leq (c_{i\sigma}|\sigma| + c_{ie}|e|)|\sigma|\,, \\ |u_d^n(\sigma)| &\leq c_\sigma|\sigma|\,, \quad \text{and} \quad |u_m^n| \leq c_m\,. \end{aligned} \tag{32}$$

It must be highlighted that the nominal control is not regarded as a disturbance and can be disregarded when the plant uncertainty is large.

Remark 2 Modulation Function Design: To satisfy $\varrho > d_0/k_o$, modulo vanishing terms due to initial conditions, the modulation function can be chosen as:

$$\varrho := (k_o + \bar{k}_p)|u_0^{av}|/k_o + \tilde{D}/k_o + \delta_\rho/k_o\,, \tag{33}$$

where

$$\tilde{D} := \bar{k}_p|u^n| + (\bar{a}_p + l_0)|\dot{y}| + \bar{k}_p\alpha_d + |\dot{\sigma}_m| + \frac{|\sigma|}{\tau_m} + \bar{\eta}\,, \tag{34}$$

*is an available norm bound for the sum $\tilde{d}_1 + \tilde{d}_2$ and $\delta_\rho > 0$ is an arbitrary small constant. In (34), we have used a norm observer for the inverse system state norm to generate $\bar{\eta} > \|C_\eta \eta\|$, modulo vanishing terms due to initial conditions. We have also considered the available norm bound function α_d for the plant input disturbance d, given in **(A1)**, and the available upper bounds $\bar{k}_p$ and $\bar{a}_p$ for k_p and a_p, respectively, both given in **(A0)**.* ∎

The main results are summarized in the following theorem.

*Theorem 1: Consider the plant represented in (5)–(8), Assumptions **(A0)**–**(A4)** and the DSSC' s algorithm and parameters in Table 1. Then, for ϕ_b (from Table 1) sufficiently large, the output tracking error is globally exponentially convergent w.r.t. a small residual set of order $\mathcal{O}(1/\phi_b^2)$, satisfying the inequality*

$$|e(t)| \leq \mathcal{O}(1/\phi_b^2) + \pi_e\,, \quad \phi_b \neq 0\,, \tag{35}$$

where π_e is an exponentially decaying term depending on the initial conditions and this residual set does not depend

TABLE 1. DSSC's dynamic functions and parameters. The free parameters are: $l_0, \phi_a, \epsilon, \delta > 0$, and $\varepsilon_i > 0$ $(i = 1, 2, 3)$.

Dynamic Functions	Dynamic Functions (Cont.)
$k_o\tau_{av} := \frac{1}{\left[\kappa_1'\hat{\phi}_1+\kappa_1\hat{\phi}_1'\right]}$	$\tau_m := \frac{\left[\kappa_1'\hat{\phi}_1+\kappa_1\hat{\phi}_1'\right]}{\left[\frac{\phi_a}{(\lvert\sigma\rvert^{1/2}+\delta)}+\phi_b\right]\left[\frac{\partial\kappa_1}{\partial e}[-l_0 e+\sigma]+\frac{\partial\kappa_1}{\partial t}+\kappa_2\hat{\phi}_1'\right]}$
$\hat{\phi}_1(\sigma) := \frac{\phi_a\sigma}{(\lvert\sigma\rvert^{1/2}+\delta)} + \phi_b\sigma$	$\hat{\phi}_1' = \phi_a\left[\frac{(\lvert\sigma\rvert^{1/2}+2\delta)}{2(\lvert\sigma\rvert^{1/2}+\delta)^2}\right] + \phi_b$
$\kappa_1 := (\kappa_a\lvert\sigma\rvert + \kappa_b\lvert e\rvert + \kappa_c)^2 + \kappa_d$	$\kappa_2 = 2\epsilon\kappa_1 + \gamma$
Design Inequalities	**Control Parameters**
$4\epsilon k_p(\gamma k_p - 4\epsilon^2) > 1$	$\gamma := \frac{(1+\varepsilon_1)}{4\epsilon k_p^2} + \frac{4\epsilon^2}{k_p}$
$\phi_b > \frac{l_0}{\epsilon}$	$\phi_b := \frac{l_0}{\epsilon} + \varepsilon_3$
$\kappa_c > \max\left\{\frac{(8\epsilon^2+2\gamma k_p)}{[4\epsilon k_p(\gamma k_p-4\epsilon^2)-1]}, \frac{(\bar{k}_{d3}\phi_b+k_\sigma)}{\phi_b^2}\right\}$	$\kappa_c := \max\left\{\frac{(8\epsilon^2+2\gamma\bar{k}_p)}{\varepsilon_1}, \frac{(\bar{k}_{d3}\phi_b+k_\sigma)}{\phi_b^2}\right\}$
$\kappa_b > \frac{(\bar{k}_{d1}\phi_b+\bar{k}_p c_{ie})}{\phi_b^2}$	$\kappa_b := \left[\frac{(\bar{k}_{d1}\phi_b+\bar{k}_p c_{ie})}{\phi_b^2}\right] + \varepsilon_2$
$\kappa_a > \max\left\{\frac{(\bar{k}_{d2}\phi_b+\bar{k}_p c_{i\sigma})}{\phi_b^2}, \frac{\kappa_b}{l_0}\right\}$	$\kappa_a := \left[\max\left\{\frac{(\bar{k}_{d2}\phi_b+\bar{k}_p c_{i\sigma})}{\phi_b^2}, \frac{\kappa_b}{l_0}\right\}\right] + \varepsilon_2$
$\kappa_d > \frac{(8\epsilon^2\gamma k_p+4\epsilon^2)}{4\epsilon k_p(\gamma k_p-4\epsilon^2)}$	$\kappa_d := \frac{(8\epsilon^2\gamma k_p+4\epsilon^2)}{4\epsilon k_p(\gamma k_p-4\epsilon^2)}$

on the initial conditions. In addition, all closed-loop signals remain uniformly bounded, finite-time escape is avoided and the sliding variable becomes identically null after some finite time $t_s \geq 0$.

Proof: For this particular case, where the functions $\tau_{av}(t)$, $\tau_m(t)$ and $k_o(t)$ are chosen according to (28) and (29), an approximation for VGSTA is synthesized during the sliding mode, and the main idea of the proof is as follows. Firstly, we prove that finite-time escape cannot occur before $\tilde{\sigma}(t) = 0$, i.e., before sliding mode takes place. Secondly, once $\tilde{\sigma} = 0$ enters in sliding motion in finite time, then the proof follows the main steps of the proof given in [19], [23] and [45]. The main difference is the introduction of the Small-Gain Theorem to deal with the approximation of the VGSTA. See Appendix D for the complete proof. ∎

1) ADDITIONAL COMMENTS

First, we recall that $\phi_b \neq 0$ in Theorem 1 allows obtaining global results. However, semi-global stability results can be achieved, when $\phi_b = 0$, since one can perform similar stability analysis as in Theorem 1, where the main difference is that the gains κ_1 and κ_2 can be designed constant around the origin of (σ, e), depending on the initial conditions.

Second, in the regulation mode case, one has that $\bar{\beta}_m$ and $\dot{y}_m$ are zero in the small-gain based analysis (Appendix D), since $k_{d5} = 0$ and $\alpha_{d2} = \alpha_{d3} = 0$ when a constant disturbance is under consideration. Thus, in this case, the tracking error e converges to zero, exponentially, and a constant disturbance is rejected.

Third, additionally to Theorem 1, prescribed finite-time convergence for the residual set can be assessed. Following the proof in Appendix D, the term $-2\epsilon\frac{1}{\mu}\frac{V}{\lambda_{max}\{P\}}$, in (55), is responsible to assure that σ and the tracking error e reach a residual set in a prescribed finite-time.

2) UNMODELLED DYNAMICS ROBUSTNESS ANALYSIS

Assume that an unmodelled dynamic represented by a transfer function of the form

$$G_\mu(\mu s) := 1 + \mu s W_\mu(\mu s)\,,$$

where $W_\mu(\mu s)$ is stable and strictly proper, is now in series with the plant input $u_p = u + u^n$, in (7), i.e.

$$u_p = u + u^n + d_\mu\,, \quad d_\mu := \mu s W_\mu(\mu s)(u + u^n)\,,$$

modulo exponentially decaying terms due to the unmodelled dynamics initial conditions. This extra term d_μ can be regarded as an additional input disturbance and **incorporated** in the input disturbance d, in (7). Recalling that $u = -u_0^{av}$ and $\tau_{av}\dot{u}_0^{av} = -u_0^{av} + u_0$, then one can write

$$d_\mu := \mu s W_\mu(\mu s)u = \mu W_\mu(\mu s)\dot{u} = \frac{\mu}{\tau_{av}} W_\mu(\mu s)(u_0^{av} - u_0)\,.$$

As some examples for the unmodelled dynamics transfer function, one has: (i) $W_\mu(\mu s) = -\frac{1}{(\mu s+1)}$ and $G_\mu(\mu s) = \frac{1}{(\mu s+1)}$; and (ii) $W_\mu(\mu s) = -\frac{(\mu s+2)}{(\mu s+1)^2}$ and $G_\mu(\mu s) = \frac{1}{(\mu s+1)^2}$. Thus, this additional disturbance d_μ is a filtered version of the averaging control u_0^{av} and the discontinuous control u_0, via a proper and stable transfer function of order $\mathcal{O}(\mu/\tau_{av})$. Thus, for μ/τ_{av} sufficiently small and despite some parasitic dynamics μ, the ideal sliding mode can still be enforced after some finite time, for the appropriate design of the modulation function.

To explain the main idea, for simplicity, consider that: (i) $u^n = 0$, (ii) τ_{av} is a constant and $\tau_m = (\lvert\sigma\rvert^{1/2}+\delta)/\kappa_1$, with κ_1 and δ being positive constants, (iii) the system has order two (no zero dynamics) and is perfectly known ($a_p^n = a_p$ and $k_p^n = k_p$), and (iv) the nominal control is given by $k_p^n u^n := -(l_0 - a_p^n)\dot{y} + \dot{\sigma}_m$. So, d_σ and the σ-dynamics, both

in (13), become

$$d_\sigma := k_p^n d \quad \text{and} \quad \dot{\sigma} = k_p^n(-u_0^{av} + d)\,, \tag{36}$$

respectively, where we have replaced u by the DSSC's control law $u = -u_0^{av}$, with u_0^{av} in (15).

Now, one can subsequently conclude that: (i) the disturbance term $\tilde{d}_1$, in (20), reduces to $\tilde{d}_1 = (-l_0\dot{y} + \dot{\sigma}_m + k_p^n d)$; (ii) $\tilde{d}_2$, in (20), reduces to $\tilde{d}_2 = (\sigma/\tau_m + l_0\dot{y} - \dot{\sigma}_m)$; (iii) $\tilde{d}_1 + \tilde{d}_2 = k_p^n d + \sigma/\tau_m$; (iv) and d_0, in (20), reduces to $d_0 = (k_o - k_p^n)u_0^{av} + k_p^n d + \sigma/\tau_m$. Let $\bar{u}_0^{av} = u_0^{av}$ be the solution of the *reduced dynamics*, resulting by replacing the discontinuous control u_0 in (15) by the *equivalent control* $u_{eq} = d_0/k_o$, obtained from the $\tilde{\sigma}$-dynamics (19). Then, one can write

$$u_{eq} = \frac{d_0}{k_o} = \left(1 - \frac{k_p^n}{k_o}\right)\bar{u}_0^{av} + \frac{k_p^n}{k_o}d + \frac{1}{k_o\tau_m}\sigma\,.$$

Now, an approximated analysis can be carried out for understanding the superior performance of the DSSC in comparison to the STA, in the presence of unmodelled dynamics. Since the averaging control $\bar{u}_0^{av}$ is an approximation of the equivalent control u_{eq}, for τ_{av} sufficiently small [46], one has that $u_{eq} \approx \bar{u}_0^{av}$ implies

$$\bar{u}_0^{av} \approx d + \frac{1}{k_p^n\tau_m}\sigma\,.$$

With $u_0^{av} = \bar{u}_0^{av}$ in (36), the closed-loop σ-dynamics can be approximated by

$$\dot{\sigma} \approx -\frac{1}{\tau_m}\sigma \approx -\frac{\kappa_1}{(|\sigma|^{1/2} + \delta)}\sigma \approx \kappa_1|\sigma|^{1/2}\mathrm{sgn}(\sigma)\,,$$

for $\delta > 0$ and small. Thus, the closed-loop σ-dynamics with the DSSC law approaches the closed-loop σ-dynamics with the standard STA, without the presence of input disturbance (with $\kappa_2 = 0$). Finally, since d incorporates the equivalent disturbance d_μ generated by the unmodelled dynamics, it becomes evident that the DSSC should outperform the corresponding STA.

B. NUMERICAL SIMULATION

The UAV's dynamic model is developed for low-velocity profiles. It means that the dynamics of the motors and the motors' drivers (ESC's) and the internal Kalman Filter dynamics (full state feedback) can be neglected, while the more relevant effects are due to the aerodynamic forces and torques.

The inner control was considered as simple as possible to be representative of the unavailable internal control loops in the DJI M600, without putting any effort into stability analysis or tuning control parameters methodologies. The consistency of the inner control loops developed here was verified first with the DJI Assistant 2 Simulator[5] and then with experimental data.

[5]The DJI Assistant 2 Simulator,[6] a program developed by DJI company that allows the users to upload flight data, calibrate vision sensors, and provide a simulator with dynamics very close to the real DJI M600 drone.

In what follows, we first present simulation results with the full UAV's dynamic model, including the aerodynamic effects and the inner control loops, and with the model (5)–(8).

The aerodynamics parameters (see Appendix A), extracted from the literature [47], are as follows: the thrust aerodynamic coefficient $k_{T_i} = 0.0024$, in Ns^2/rad, the aerodynamic torque coefficient $c_\tau = 0.57$, in $mrad/s^2$, the matrix coefficient $K_{F_d} = \mathrm{diag}\left(\begin{bmatrix}0.03 & 0.03 & 0.015\end{bmatrix}\right)$ of the drag force on the structure, in Ns^2/m^2, and the matrix coefficient $K_{F_{di}} = \mathrm{diag}\left(\begin{bmatrix}1 & 1 & 1\end{bmatrix}\right)(8 \times 10^{-6})$ of the propeller drag force, in $Ns^2/(mrad)$.

To simplify the control allocation, we consider a quadrotor with the same weight, size, and geometry as the DJI M600. The UAV's parameters can be summarized as follows: the number of rotors $n_r = 4$, the directions of rotation $s_1 = 1$, $s_2 = -1$, $s_3 = 1$ and $s_4 = -1$, the propeller half length $r = 0.1$m (radius), the rotor displacement measured from the center of mass and along the horizontal plane $d = 0.57$m, the UAV's inertia tensor (in kgm^2) $I_b = \mathrm{diag}\left(\begin{bmatrix}0.4 & 0.4 & 0.74\end{bmatrix}\right)$, the UAV's mass $\mathcal{M} = 10.9$kg, the propeller hub inertia tensor (in kgm^2) $I_i = \mathrm{diag}\left(\begin{bmatrix}0.01 & 0.01 & 0.5 \times 10^{-5}\end{bmatrix}\right)$. The arm length is, thus, $L = \sqrt{d^2 + h^2} = 0.57$m. The inner control loops are based on state feedback linearization-based controllers with feedforward and integral actions, with control gains: $k_p^z = 0$, $k_d^z = 1$, $k_p^\psi = 0.2$, $k_d^\psi = 1$, $k_p^\phi = 60$, $k_d^\phi = 15$, $k_p^\theta = 60$, $k_d^\theta = 15$, $k_p^x = 0$, $k_d^x = 1$, $k_p^y = 0$ and $k_d^y = 1$.

All initial conditions were set at zero except the drone position $p_x(0) = 40$m, $p_y(0) = 10$m and $p_z(0) = 10$m, and yaw angle $\psi(0) = (\pi/4)$rad (45deg). The desired trajectories are: $p_{x_d}(t) = 20\sin(2\pi/40t)$, $p_{y_d}(t) = 20\cos(2\pi/40t)$, $p_{z_d}(t) = 3\sin(2\pi/60t) + 5$, and $\psi_d(t) = -(\pi/4)\sin(2\pi/40t) + \pi/4$. For all four degrees of freedom, the DSSC algorithm is implemented with τ_{av} constant and with the state-dependent functions

$$k_o(t) := \kappa_o(|\sigma(t)|^{1/2} + \delta)\,, \quad \tau_m(t) := \kappa_m(|\sigma(t)|^{1/2} + \delta)\,,$$

where $\delta = 1$ and $\kappa_m = 4.0166$. Moreover, for the x and y subsystems, were selected the parameters $\kappa_o = 110.651$, $\tau_{av} = 0.03$ and $\varrho = 1.5$. For the z-subsystem, were selected $\kappa_o = 55.3255$, $\tau_{av} = 0.06$ and $\varrho = 0.5$. For the ψ-subsystem, were selected $\kappa_o = 55.3255$, $\tau_{av} = 0.06$ and $\varrho = 0.15$. The other DSSC's parameter is $l_0 = 0.2$, for all subsystems.

Now, we consider two cases.

Case 1: the full UAV dynamic (1), see also Figure 1, with a constant wind velocity $v_w = \begin{bmatrix}8 & -8 & 8\end{bmatrix}^T$*, in m/s, added after* $t = 20$*s. This effect can be observed only for the full UAV's model which incorporates the aerodynamic drag terms (blue lines).*

Case 2: the simplified UAV model (6)–(8), without inverse dynamics and with a constant input disturbance d added in each subsystem (5)–(8), after $t = 20$*s:* $d = -0.8$*, for the x-subsystem;* $d = 0.8$*, for the y-subsystem;* $d = 0.2$*, for the z-subsystem; and* $d = 0.1$*, for the* ψ*-subsystem.*

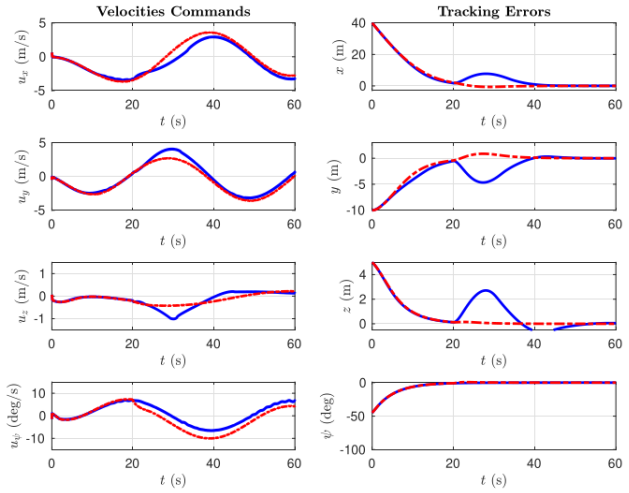

FIGURE 3. Simulations of the DSSC with the full UAV dynamic model (blue line) and with the simplified model (red line). The control efforts are in the left column, while the tracking errors are given in the right column.

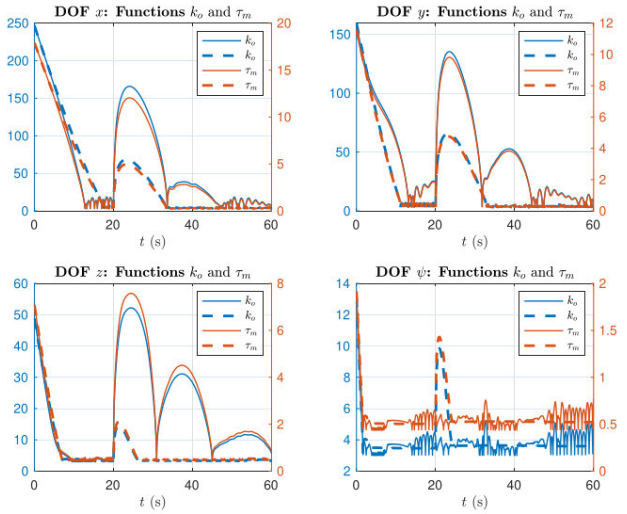

FIGURE 4. Simulations of the DSSC with the full UAV dynamics model (solid line) and with the simplified model (dash line). The time history of $k_o(t)$ and $\tau_m(t)$ are illustrated for the 4 degree of freedom.

For simplicity, we set $a_p^n = a_p = 1$ and $k_p^n = k_p = 1$ for the four subsystems in Case 2. This lead to a simplified nominal control, which can be chosen as

$$u^n := -c_e e - c_\sigma \sigma - c_{m1}\dot{y}_m - c_{m2}\ddot{y}_m\,, \tag{37}$$

with constants $c_e = (a_p^n - l_0)l_0/k_p^n, c_{m1} = -a_p^n, c_{m2} = -1$ and a time-varying coefficient $c_\sigma(t) = (l_0 - a_p^n + 1/\tau_m(t))/k_p^n$, which satisfies $|c_\sigma(t)| \leq (|l_0 - a_p^n| + 1/(\kappa_m\delta))/k_p^n$. This nominal control was also considered in Case 1.

In the left column of Figure 3, one can see the velocity command reactions to compensate for the disturbances, after $t = 20$s. Recall that the disturbances are different for the full UAV dynamic (wind disturbance) and for the UAV model dynamics (5)–(8) (input disturbance d). However, before the disturbances ($t < 20$), both tracking errors' behavior (right column) is very similar, except for a residual oscillation in the DSSC control signal (left column), when applied to the full UAV model case (blue line), due to the inner control loops (unmodelled dynamics effect).

Figure 4 illustrates the time-varying behavior of the state-dependent functions $k_o(t)$ and $\tau_m(t)$, where both increase when the disturbance acts after $t = 20$s.

In what follows, we study the robustness of the DSSC scheme w.r.t. unmodelled dynamics in comparison to the STA. Consider the STA and the DSSC applied to the full UAV model, without wind disturbance. For the x and y subsystems, were selected the parameters $\tau_{av} = 0.03$ and $\varrho = 0.375$. For the z-subsystem, were selected $\tau_{av} = 0.06$ and $\varrho = 0.125$. For the ψ-subsystem, were selected $\tau_{av} = 0.06$ and $\varrho = 0.0375$. The other DSSC's parameters (for all subsystems) are: $\delta = 2$ for k_o, $\delta = 0.0025$ for τ_m, and $l_0 = 0.2$.

For the x, y, and ψ subsystems, the STA's gain $\kappa_2 = 100$ provokes significant oscillations when compared with the DSSC equivalent implementation, see Figure 5. For the z subsystem, in particular, this effect is attenuated since the inner control performs perfect decoupling and feedback

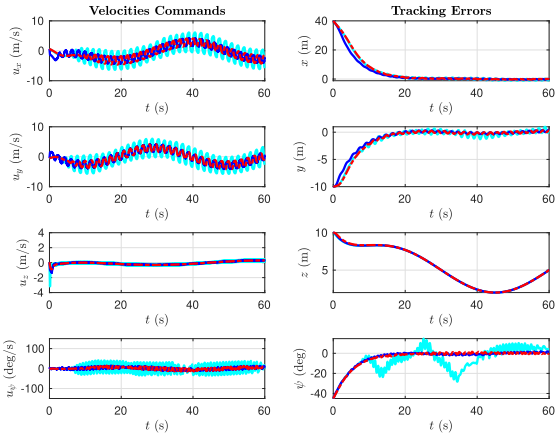

FIGURE 5. Simulations of the DSSC (blue line) and the STA (red line) with the full UAV dynamic model.

linearization. For small values of κ_2, both controllers have similar behavior (curves not shown).

C. EXPERIMENTAL RESULTS

The desired trajectory for the commercial DJI M600 Pro hexacopter was created to be executed in the field next to the laboratory (a soccer field), which is free of obstacles and barriers, at the Federal University of Rio de Janeiro. The path was obtained by using the Path Sketch Interface (PSI), a Python interface with a satellite image from the area of interest that allows the users to choose the desired points, see Figure 6. Then, a Matlab script converts the georeferenced points to the east-north-up (ENU) reference system and generates a smooth trajectory version using a differentiable parametric curves approach. Finally, the controllers are developed using the Robotic Operation System (ROS) and C++. The ROS control node runs on an onboard Raspberry Pi 4 and loads the trajectory information generated by the Matlab script to execute the mission.

FIGURE 6. Desired trajectory obtained via the developed Path Sketch Interface (PSI).

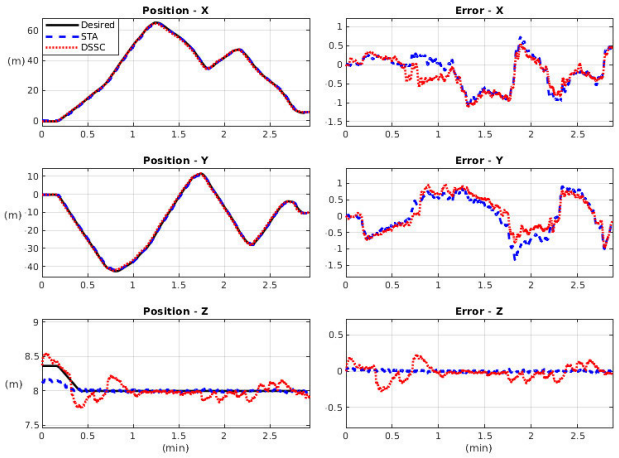

FIGURE 7. Field Test. Trajectory tracking performance under STA (dash blue) and DSSC (dot red) and the trajectory error along the three axes. The desired trajectory is illustrated in black.

Our main purpose here is to experimentally evaluate the DSSC scheme in a real environment with the presence of real wind disturbances while ratifying that its closed-loop behavior during sliding mode approaches the STA.

It must be highlighted that the same code implemented for all control laws works for the real-time implementation embedded in the UAV computer, as well as, in the simulator developed based on the full UAV model (1) and in the DJI Assistant 2 Simulator. The controllers were satisfactory tested with wind disturbance in the DJI Assistant 2 considering the wind speed of 8 m/s for the $x-y$ axes and 2 m/s for the z axis. The results are omitted due to lack of space.

After the test in the simulator, the controllers were tested in a representative environment within the Federal University of Rio de Janeiro, a soccer field (Figure 6), on the same day (April 20, 2022) and with the same wind conditions, i.e., a moderate wind with speed ranging from 5 m/s to 8 m/s, according to the anemometer installed in the field.

It was assumed that the nominal values for the uncertain parameters are (for all channels): $a_p^n = k_p^n = 2$. The same DSSC's control parameters, as well as, the STA's parameters are used in all subsystems (x, y, x, and ψ). It was verified that a constant modulation function ($\varrho(t) = 4$) was enough to deal with the uncertainties and the relative degree one output variable σ, in (10), was implemented with $l_0 = 2$.

The STA control was tuned to ensure acceptable performance in the real scenario, resulting in $\kappa_2 = 0.035$ and $\kappa_1 = 0.075$. The DSSC was implemented with

$$\tau_{av}(t) := \frac{2}{k_o\kappa_1}|\sigma(t)|^{1/2} + \delta\,, \quad \tau_m(t) := \frac{\kappa_1}{2\kappa_2}|\sigma(t)|^{1/2} + \delta\,,$$

$k_o = 10$ and $\delta = 0.1$, for all subsystems. The control gains of the STA and the DSSC's parameters were increased in the experiments in comparison to the gains used in the DJI Assistant 2 simulator.

Figure 7 shows the closed-loop tracking performance for both controls. To put in evidence the influence of the STA's gains, we have left the gain of the STA altitude control (z axis) at the same level as in the simulation. This effect is observed at the bottom of Figure 7, where the tracking error using the STA (red line) is significantly greater than the error using the DSSC scheme (blue line). The left-bottom xy plot appearing in Figure 6 illustrates the path tracking in the xy axes. The corresponding control efforts are very similar, ratifying that the DSSC closed-loop behavior during sliding mode approaches the STA, but the curves are not shown to save space.

VI. CONCLUSION

A modification in the previous Smooth Sliding Control was proposed, named Dynamic Smooth Sliding Control (DSSC), which incorporates functions in the predictor and the averaging filter depending on the output tracking error e and its time derivative. The internal predictor and averaging filter are responsible for ensuring ideal sliding mode (in an internal variable) and smooth control effort, respectively, leading to chattering avoidance.

Global stability properties were achieved, leading to exact output regulation and exponential convergence of the output tracking error to a residual set depending on the steady-state value of the smooth filter pass-band (practical tracking).

Experimental evaluation with a commercial hexacopter corroborated that the new design based on the class of plants considered here, in fact, is robust to unmodelled dynamics and is feasible to be digitally implemented with a regular sampling rate.

A. DISCUSSION AND FUTURE WORKS

It was verified that the DSSC can be designed so that the synthesized control law during sliding mode generates a family of controllers, in particular, approximations for the standard and variable gain STA. This has motivated the complete stability analysis of the DSSC inspired by the STA analysis.

Improvement was obtained in the practical implementation where discretization, for instance, generates numerical chattering even for the relative degree one case. Since sliding motion can occur even with still large output error, so that the modulation function is also large, a time-varying passband (inversely proportional to e) resulted in a practical smoother control action when compared with the original SSC, maintaining at least the same level of tracking precision. The robustness concerning unmodelled dynamics (parasitic) was inherited from the intrinsic robustness with respect to the smooth filter. Moreover, numerical simulations with a UAV dynamic model including aerodynamics effects and inner controllers and with the DJI Assistant 2 simulator, also illustrated that the class of plants fits the application.

Investigation of alternative state-dependent functions for the DSSC, closed-loop stability analysis in the presence of parasitic or unmodelled dynamics, and a methodology to adapt the actual UAV simulation model for other types of UAVs are under development.

APPENDIX A UAV MODEL: AERODYNAMIC TERMS AND DISTURBANCES

In the UAV dynamic model (see also Figure 1), the term τ_{dist} and the parameter $\mathcal{J}$ are defined as

$$\tau_{dist} := \left[I_z\Omega_y \textstyle\sum_{i=1}^{n_r} \dot{\theta}_i \; -I_z\Omega_x \sum_{i=1}^{n_r} \dot{\theta}_i \; I_z \sum_{i=1}^{n_r} \ddot{\theta}_i \right]^T ,$$

and

$$\mathcal{J} = \text{diag}\left(\left[n_r I_{xy} + I_{bx} \;\; n_r I_{xy} + I_{by} \;\; n_r I_z + I_{bz} \right] \right) ,$$

where the inertia tensor of the i-th propeller hub (propeller plus motor), represented in $\mathcal{E}_i$ (the i-th propeller frame), is a diagonal matrix $I_i = \text{diag}\left(\left[I_{xi} \; I_{yi} \; I_{zi} \right] \right)$, with $I_{xi} = I_{yi} = I_{xy}$ and $I_{zi} = I_z$ $(\forall i)$; and the inertia tensor of the UAV's structure, represented in $\mathcal{E}_b$, is a diagonal matrix $I_b = \text{diag}\left(\left[I_{bx} \; I_{by} \; I_{bz} \right] \right)$.

The following terms incorporate all drag effects on the UAV:

$$F_{drag} := \sum_{i=1}^{n_r} F_{di} + F_d \,, \quad \text{and} \quad \tau_{drag} := \sum_{i=1}^{n_r} (p_{bi} \times R^T F_{di}) \,,$$

where p_{bi} is the position vector of the origin of the propeller frame relative to the origin of the body frame (represented in the body frame), and for the control allocation, $M := \sum_{i=1}^{n_r} (p_{bi} \times T_i) + \sum_{i=1}^{n_r} \tau_{di}$ is the *net moment*, and $f = \sum_{i=1}^{n_r} f_i$ is the *net thrust magnitude*. The aerodynamic terms are defined in what follows. The **Propeller Aerodynamic Thrust** is given by T_i (body frame) with the thrust magnitude $f_i := k_{T_i}\dot{\theta}_i^2$ proportional to the rotor spin rate square via Rayleigh's equation, where $k_{T_i} > 0$ is the thrust aerodynamic constant and $\dot{\theta}_i$ is the i-th propeller spin rate. The **Propeller Aerodynamic Drag Torque** is denoted by τ_{di} (body frame), with magnitude $|\tau_{di}| = c_\tau k_{T_i}\dot{\theta}_i^2$, torque direction $s_i = \text{sgn}(\tau_{di}) = -\text{sgn}(\dot{\theta}_i)$ and aerodynamic torque constant $c_\tau > 0$. The **Propeller Aerodynamic Drag Force** is given by $F_{di} := -K_{F_{di}} |\dot{\theta}_i| \, v_{ri}$ (inertial frame), where $v_{ri} := v_i - v_w$ is the propeller air-relative velocity, v_i is the linear velocity of the i-th propeller frame, v_w is the wind velocity, both represented in the inertial frame and $K_{F_{di}} > 0$ is the propeller aerodynamic drag force matrix coefficient. Finally, $F_d := -RK_{F_d}R^T v_r \, \|v_r\|$ is the **UAV Aerodynamics Drag Force on the Structure**, where $v_r := v - v_w$ is the air-relative velocity, and $K_{F_d} > 0$ is the structure aerodynamic drag force matrix coefficient. ∎

APPENDIX B NORMAL FORM

In this section, the development of the normal form (3)–(4) is provided. From (2), one has that

$$(\ddot{\nu} - \ddot{u}) = -k_p(\dot{\nu} - \dot{u}) - k_i(\nu - u) + \left[\dot{\mathcal{D}} - \ddot{u} \right] , \tag{38}$$

or, equivalently,

$$\ddot{\nu} + k_p\dot{\nu} + k_i\nu = k_p\dot{u} + k_iu + \dot{\mathcal{D}} \,. \tag{39}$$

Reminding that $d = \frac{s}{(k_ps+k_i)}\mathcal{D}$, one can further write $k_p\dot{d} + k_id = \dot{\mathcal{D}}$, leading to

$$\ddot{\nu} + k_p\dot{\nu} + k_i\nu = k_p(\dot{u} + \dot{d}) + k_i(u + d) \,. \tag{40}$$

Now, with the change of coordinate

$$\eta := -\frac{k_p^2}{k_i^2}\left[\dot{\nu} + \frac{(k_p^2 - k_i)}{k_p}\nu - k_p(u + d) \right] , \tag{41}$$

one has

$$\begin{aligned} \dot{\eta} &:= -\frac{k_p^2}{k_i^2}\left[\ddot{\nu} + \frac{(k_p^2 - k_i)}{k_p}\dot{\nu} - k_p(\dot{u} + \dot{d}) \right] \\ &= -\frac{k_p^2}{k_i^2}\left[-k_i\nu - \frac{k_i}{k_p}\dot{\nu} + k_i(u + d) \right] \\ &= \frac{k_p}{k_i}\left[k_p\nu + \dot{\nu} - k_p(u + d) \right] , \end{aligned}$$

where the last two equalities comes from (40). In addition, from (41) one can write

$$a_\eta\eta := \frac{k_p}{k_i}\left[\dot{\nu} + k_p\nu - k_p(u + d) \right] - \nu \,,$$

with $a_\eta := -\left[\frac{k_i}{k_p} \right]$ and obtain (3), with $b_\eta = 1$. Finally, one can further write from (41) that

$$\dot{\nu} = -\frac{k_i^2}{k_p^2}\eta + k_p(u + d) - \frac{(k_p^2 - k_i)}{k_p}\nu \,, \tag{42}$$

which is precisely (4), with $a_p = \left[\frac{k_p^2 - k_i}{k_p} \right]$ and $c_\eta = \left[\frac{k_i}{k_p} \right]^2$. ∎

APPENDIX C SOME CASES OF DSSC'S SYNTHESIZED CONTROLLERS

To illustrate some of those possibilities, consider the four cases illustrated in Table 2, where for simplicity, we let $k_o\tau_{av}$, τ_m, g_1 and g_2 be functions of σ, only. Thus, $\frac{\partial g_1}{\partial e} = \frac{\partial g_1}{\partial t} = 0$ and, from (23), one has

$$\left[\frac{1}{k_o\tau_{av}} \right] = g_1'\sigma + g_1 \,, \quad \text{and} \quad \left[\frac{1}{k_o\tau_{av}\tau_m} \right] = g_2 \,. \tag{43}$$

TABLE 2. Some special cases of synthesized controllers (PI, standard STA, and two approximations for the standard STA). For the standard STA case, since $k_o\tau_{av}$ and τ_m tend to zero as $\sigma \to 0$, then the DSSC's averaging filter and predictor dynamic become very fast, leading to an undesired stiff problem. To avoid this problem, the idea is to use approximations $\hat{\phi}_1$ and $\hat{\phi}_2$, for ϕ_1 and ϕ_2, respectively. For the first approximation for the STA, the DSSC's state-dependent functions are well defined for all finite σ, and one has that $\hat{\phi}_1 \to \phi_1 = |\sigma|^{1/2}\text{sgn}(\sigma)$ and $\hat{\phi}_2 = \hat{\phi}_1'\hat{\phi}_1 \to \phi_2 = \phi_1'\phi_1 = \text{sgn}(\sigma)/2$, as $\delta \to 0$. As an alternative, in the second approximation for the STA, another choice for $\hat{\phi}_2$ can be explored, even if not satisfying the relationship $\hat{\phi}_2 = \hat{\phi}_1'\hat{\phi}_1$. However, one still have $\hat{\phi}_2 \to \phi_2 = \phi_1'\phi_1 = \text{sgn}(\sigma)/2$, as $\delta \to 0$, but $\hat{\phi}_2 \neq \hat{\phi}_1'\hat{\phi}_1$. For all cases, κ_1 and κ_2 are positive constant gains, and $\delta > 0$ is an arbitrarily small constant.

Controller	g_1	g_2	$\hat{\phi}_1$	$\hat{\phi}_2$	State-Dependent Functions
PI Control	cte	cte	$\ldots$	$\ldots$	$k_o\tau_{av} = 1/g_1, \tau_m = g_1/g_2$
Standard STA	$\kappa_1\lvert\sigma\rvert^{-1/2}$	$\frac{\kappa_2}{2}\lvert\sigma\rvert^{-1}$	$\phi_1 := \sigma\lvert\sigma\rvert^{-1/2}$	$\phi_2 := \phi_1\phi_1'$	$k_o\tau_{av} = \frac{1}{\kappa_1\phi_1'} = \frac{2}{\kappa_1}\lvert\sigma\rvert^{1/2}$ and $\tau_m = \frac{\kappa_1\phi_1'\sigma}{\kappa_2\phi_2} = \frac{\kappa_1\sigma}{\kappa_2\phi_1} = \frac{\kappa_1}{\kappa_2}\lvert\sigma\rvert^{1/2}$
Approx. STA	$\kappa_1\hat{\phi}_1\sigma^{-1}$	$\kappa_2\hat{\phi}_2\sigma^{-1}$	$\left[1 - \frac{\delta\ln\left(\frac{\lvert\sigma\rvert^{1/2}+\delta}{\delta}\right)}{\lvert\sigma\rvert^{1/2}}\right]\phi_1$	$\hat{\phi}_1\hat{\phi}_1'$	$k_o\tau_{av} = \frac{1}{\kappa_1\hat{\phi}_1'}$, $\tau_m = \frac{\kappa_1\hat{\phi}_1'\sigma}{\kappa_2\hat{\phi}_2}$, $k_o\tau_{av} = \frac{2}{\kappa_1}(\lvert\sigma\rvert^{1/2}+\delta)$ and $\tau_m = \frac{\kappa_1}{\kappa_2}\lvert\sigma\rvert^{1/2}\left[1 - \frac{\delta\ln\left(\frac{\lvert\sigma\rvert^{1/2}+\delta}{\delta}\right)}{\lvert\sigma\rvert^{1/2}}\right]^{-1}$
Approx. STA	$\kappa_1\hat{\phi}_1\sigma^{-1}$	$\kappa_2\hat{\phi}_2\sigma^{-1}$	$\left[1 - \frac{\delta\ln\left(\frac{\lvert\sigma\rvert^{1/2}+\delta}{\delta}\right)}{\lvert\sigma\rvert^{1/2}}\right]\phi_1$	$\frac{\sigma}{2(\lvert\sigma\rvert^{1/2}+\delta)^2}$	$k_o\tau_{av} = \frac{1}{\kappa_1\hat{\phi}_1'}$, $\tau_m = \frac{\kappa_1\hat{\phi}_1'\sigma}{\kappa_2\hat{\phi}_2}$, $k_o\tau_{av} = \frac{2}{\kappa_1}(\lvert\sigma\rvert^{1/2}+\delta)$ and $\tau_m = \frac{\kappa_1}{\kappa_2}(\lvert\sigma\rvert^{1/2}+\delta)$

From Table 2, for the plant (5)–(7), the synthesized DSSC can result in an approximation for the STA [16], [18]. This approximation acts like a gain reducer near the origin of the error system state-space (σ, e), thus, improving the robustness concerning unmodelled dynamics. In what follows, we point out some remarkable features of the synthesized DSSC.

From a theoretical point of view, this synthesized approximation becomes exactly the standard STA, as $\delta \to 0$. In addition, when the pass-band of the averaging filter tends to infinity, the closed-loop dynamics with the synthesized DSSC law approaches the closed-loop dynamics with the STA, *in the absence of unmodelled dynamics*, as described in the approximated analysis in Section V-A2.

On the other hand, from a practical point of view, small values for δ are enough to obtain similar results as the standard STA, far away from the origin, while assuring acceptable input disturbance rejection capabilities near the origin.

In addition, it should be highlighted that the initial value of the DSSC's control effort can be arbitrary chosen (e.g., at zero) by setting the initial condition of the averaging filter.

APPENDIX D PROOF OF THEOREM 1

The proof is carried out in two parts: before and after sliding mode takes place.

PART A: ANALYSIS DURING THE REACHING PHASE

From the $\tilde{\sigma}$-dynamics (19), one can obtain $\dot{\tilde{\sigma}}\tilde{\sigma} \leq -1/\tau_m\tilde{\sigma}^2 - \delta_\varrho|\tilde{\sigma}| \leq -\delta_\varrho|\tilde{\sigma}|$, since the modulation function was designed in (33) to overcome the disturbance d_0/k_o, i.e., to satisfy $\varrho > |d_0|/k_o + \delta_\varrho/k_o$. The last inequality established the well-known δ_ρ-*reachability condition* [48]. Now, one can write

$$\dot{\tilde{\sigma}}\tilde{\sigma} = \frac{1}{2}\frac{d}{dt}\left[\tilde{\sigma}^2(t)\right] \leq -\delta_\varrho|\tilde{\sigma}(t)|\,, \tag{44}$$

and integrating (44) from t_0 to $t \in [t_0, t_M)$, with $t \leq T_s$ and $T_s := t_0 + |\tilde{\sigma}(t_0)|/\delta_\varrho$, it follows that

$$|\tilde{\sigma}(t)| \leq -\delta_\varrho(t - t_0) + |\tilde{\sigma}(t_0)| \leq |\tilde{\sigma}(t_0)|\,,$$

$\forall t \in [t_0, t_M)$ and $t \leq T_s$. It is clear that $\tilde{\sigma}(t_0) = 0$ implies sliding mode at the manifold $\tilde{\sigma}(t) \equiv 0$, starting from the beginning, i.e., $\forall t \in [t_0, t_M)$, since $T_s = t_0 + |\tilde{\sigma}(t_0)|/\delta_\varrho = t_0$ and the δ_ρ-*reachability condition* (44) is satisfied. In this case, finite-time escape cannot occur before sliding mode takes place. Thus, from now on, assume that $\tilde{\sigma}(t_0) \neq 0$.

Assuming that t_M is finite, then there exists a finite t^* ($t_0 < t_M < t^*$) such that some close-loop signal escapes at $t = t^*$. Moreover, aiming to prove that finite-time escape cannot occur before sliding mode takes place, assume that $\tilde{\sigma}(t) \neq 0$, $\forall t \in [t_0, t^*]$.

Due to the unboundedness observability property of the closed-loop system, finite-time escape can occur if and only if the output $\sigma = \dot{e} + l_0 e$ escapes in finite-time. In addition, since the δ_ρ-*reachability condition* holds, then $\tilde{\sigma}$ is uniformly norm bound in the time interval $[t_0, t^*]$.

Then, $\hat{\sigma}(t) = \sigma(t) - \tilde{\sigma}(t)$ must also escapes at $t = t^*$ and $\lim_{t\to t^*}|\hat{\sigma}(t)| = \infty$. However, at this point, $\hat{\sigma}$ can escape to infinity while oscillating around zero (and switching sign), or monotonically with a fixed sign. The first case does not occur. Indeed, since ϱ in (33) satisfies $\varrho \geq |u_0^{av}|$, then the term $[-u_0^{av} + u_0] = [-u_0^{av} + \varrho\text{sgn}(\tilde{\sigma}(t_0))]$, appearing in the predictor $\hat{\sigma}$-dynamics (18), has the same sign as $\tilde{\sigma}(t_0)$, where we have used the fact that $\text{sgn}(\tilde{\sigma}(t)) = \text{sgn}(\tilde{\sigma}(t_0))$. Therefore, one can write the $\hat{\sigma}$-dynamics as

$$\tau_m(t)\dot{\hat{\sigma}} = -\hat{\sigma} + \tau_m(t)k_o(t)|-u_0^{av} + u_0|\text{sgn}(\tilde{\sigma}(t_0))\,,$$

and $\hat{\sigma}$ cannot escape in finite-time oscillating and crossing zero, since the input of the $\hat{\sigma}$-dynamics has the fixed sign $\text{sgn}(\tilde{\sigma}(t_0))$ in the interval $[t_0, t^*]$. So, there exists $T_0 \in [t_0, t^*]$

such that $\hat{\sigma}(t) \neq 0$, $\forall t \in [T_0, t^*]$, escaping monotonically with a fixed sign.

However, for $\text{sgn}(\tilde{\sigma}(t_0)) = 1$, one has $\tilde{\sigma}(t) > 0$, $\sigma(t) > \hat{\sigma}(t)$, $\lim_{t\to t^*} \hat{\sigma}(t) = +\infty$ and the strictly inequality $q(t) := \frac{\sigma(t)}{\hat{\sigma}(t)} > 1$ holds. Now, note that the quotient $q(t) = \frac{\sigma(t)}{\hat{\sigma}(t)} = 1 + \frac{\tilde{\sigma}(t)}{\hat{\sigma}(t)}$ and $\lim_{t\to t^*} \frac{\tilde{\sigma}(t)}{\hat{\sigma}(t)} = 0$, where we have used the facts that $\tilde{\sigma}(t)$ is uniformly norm-bounded in the closed time interval $[t_0, t^*]$ and $\lim_{t\to t^*} \hat{\sigma}(t) = +\infty$. Thus, one can further write $\lim_{t\to t^*} q(t) = 1$, which is a contradiction since $q(t)$ is strictly greater than one, $\forall t \in [t_0, t^*]$. For $\text{sgn}(\tilde{\sigma}(t_0)) = -1$, one has $\tilde{\sigma}(t) < 0$, $k_\sigma \sigma(t) < \hat{\sigma}(t)$, $\lim_{t\to t^*} \hat{\sigma}(t) = -\infty$ and the inequality $q(t) := \frac{k_\sigma \sigma(t)}{\hat{\sigma}(t)} < 1$ holds in the closed time interval $[t_0, t^*]$. Analogously, the quotient $q(t)$ also satisfies $\lim_{t\to t^*} q(t) = 1$, which again is a contradiction since $q(t)$ is strictly less than one, $\forall t \in [t_0, t^*]$.

Finally, one can conclude that sliding mode occurs before any closed-loop signal escapes in finite time. However, finite-time escape is not precluded after sliding mode takes place. To complete the proof, we will evoke the Small Gain Theorem.

PART B: ANALYSIS IN SLIDING MODE

From **Part (a)**, there exists a finite time $t_s \in [0, t_M)$ such that, $\forall t \in [t_s, t_M)$, sliding mode occurs, i.e., the sliding variable $\tilde{\sigma}(t)$ becomes identically null.

During sliding mode, the synthesized DSSC law is given by $\bar{u} = \hat{u}_{vgsta} + C_s$, with $C_s := \bar{u}(t_s) + \kappa_1(t_s)\hat{\phi}_1(t_s)$ and $\hat{u}_{vgsta}$ in (27), leading to

$$\bar{u}(t) = -\kappa_1(t)\hat{\phi}_1(t) - \int_{t_s}^{t} \kappa_2(\tau)\hat{\phi}_2(\tau)d\tau + C_s\,. \tag{45}$$

Now, in what follows, consider the signal and the norm bounds given in Appendix E. Then, with $u = \bar{u}$, defining the auxiliary variable

$$z := -k_p \int_{t_s}^{t} \kappa_2(\tau)\hat{\phi}_2(\sigma(\tau))d\tau + \sigma_a + k_p C_s\,, \tag{46}$$

with σ_a in (64) and $\dot{\sigma}_a$ in (65), the **closed-loop system during sliding mode** can be written as ($\forall t \in [t_s, t_M)$)

$$\dot{e} = -l_0 e + \sigma\,, \tag{47}$$

$$\dot{\sigma} = -k_p\kappa_1\hat{\phi}_1 + \beta_1 + z\,, \tag{48}$$

$$\dot{z} = -k_p\kappa_2\hat{\phi}_2 + \beta_2 + \beta_e + \beta_m\,, \tag{49}$$

with β_1 in (63), β_2 in (68), β_e in (67), β_m in (66), where we have used the fact that C_s is a constant. As in [23], an additional transformation will be useful for the convergence analysis and gains design. Defining

$$\zeta := \begin{bmatrix} \zeta_1 & \zeta_2 \end{bmatrix} = \begin{bmatrix} \hat{\phi}_1 & z \end{bmatrix}\,,$$

and noting that $\dot{\zeta}_1 = \hat{\phi}_1'\dot{\sigma}$ and $\hat{\phi}_2 = \hat{\phi}_1'\hat{\phi}_1$, we rewrite (48) and (49) as $\dot{\zeta}_1 = \hat{\phi}_1'\left[-(k_p\kappa_1 - \alpha_1)\hat{\phi}_1 + z\right]$ and $\dot{\zeta}_2 = \hat{\phi}_1'\left[-(k_p\kappa_2 - \alpha_2)\hat{\phi}_1\right] + \beta_e + \beta_m$, respectively, where α_1 and α_2 are treated as uncertain disturbances functions defined by

$$\alpha_1\hat{\phi}_1 := \beta_1 \quad \text{and} \quad \alpha_2\hat{\phi}_2 := \beta_2\,, \quad \forall\sigma \neq 0\,, \tag{50}$$

and $\alpha_1 = \alpha_2 = 0$, for $\sigma = 0$. Finally, the closed-loop dynamics during sliding mode can be written in the compact form:

$$\dot{e} = -l_0 e + \sigma\,, \tag{51}$$

$$\dot{\zeta} = \hat{\phi}_1' A(\sigma, e, t)\zeta + B(\beta_e + \beta_m)\,, \tag{52}$$

where

$$A(\sigma, e, t) := \begin{bmatrix} -(k_p\kappa_1 - \alpha_1) & 1 \\ -(k_p\kappa_2 - \alpha_2) & 0 \end{bmatrix}\,, \quad B := \begin{bmatrix} 0 & 1 \end{bmatrix}^T\,,$$

β_e in (67), β_m in (66) and α_1 and α_2 in (50). Similarly to [23], consider the Lyapunov function candidate

$$V(\zeta) := \zeta^T P\zeta\,, \quad P := \begin{bmatrix} \gamma k_p & -2\epsilon \\ -2\epsilon & 1 \end{bmatrix}\,, \tag{53}$$

where $\gamma, \epsilon > 0$ are design constants and k_p is one of the uncertain plant parameter (thus, P is an uncertain matrix). Then, one can obtain

$$\dot{V} = -\hat{\phi}_1'\zeta^T Q\zeta + 2\zeta^T PB(\beta_e + \beta_m)\,, \tag{54}$$

where $Q := -\left(A^T P + PA\right)$. The variable gains are designed (Table 1) to assure that matrix $Q - 2\epsilon I$ is positive definite, see Appendix F. Now, with $Q - 2\epsilon I > 0$ and reminding that $\hat{\phi}_1' = \phi_a\left[\frac{(|\sigma|^{1/2}+2\delta)}{2(|\sigma|^{1/2}+\delta)^2}\right] + \phi_b$, then one can write $-\hat{\phi}_1'\zeta^T Q\zeta \leq -2\epsilon\frac{1}{\mu}\|\zeta\|^2 - 2\epsilon\phi_b\|\zeta\|^2$ and

$$-\hat{\phi}_1'\zeta^T Q\zeta \leq -2\epsilon\frac{1}{\mu}\frac{V}{\lambda_{max}\{P\}} - 2\epsilon\phi_b\frac{V}{\lambda_{max}\{P\}}\,, \tag{55}$$

where

$$\mu := \frac{2}{\phi_a}\left[\frac{(|\sigma|^{1/2} + \delta)^2}{(|\sigma|^{1/2} + 2\delta)}\right]\,, \quad \phi_a\,, \delta > 0\,,$$

and the Rayleigh quotient was applied. To simplify the analysis at the cost of being more conservative and losing the capability of achieving the prescribed finite-time convergence for a residual set, we disregard this negative term $-2\epsilon\frac{1}{\mu}\frac{V}{\lambda_{max}\{P\}}$ in (55), leading to

$$-\hat{\phi}_1'\zeta^T Q\zeta \leq -2\epsilon\phi_b\frac{V}{\lambda_{max}\{P\}}\,. \tag{56}$$

In addition, from (71) and (70), one can write $|\beta_e + \beta_m| \leq \|C_\eta A_\eta\|\|\eta\| + \kappa_e|e| + \bar{\beta}_m$, where $\bar{\beta}_m := \bar{k}_p k_{d5}|y_m| + \bar{k}_p|\dot{u}_m^n| + |\ddot{\sigma}_m| + (l_0 + \bar{a}_p)|\ddot{y}_m| + (\bar{k}_p k_{d4} + \|C_\eta B_\eta\|)|\dot{y}_m| + \bar{k}_p(\alpha_{d2} + \alpha_{d3})$. Then, the term $2\zeta^T PB(\beta_e + \beta_m)$ in (54) satisfies

$$|2\zeta^T PB(\beta_e + \beta_m)| \leq \frac{2\|PB\|}{\lambda_{min}^{1/2}\{P\}}V^{1/2}(\|C_\eta A_\eta\|\|\eta\| + \kappa_e|e| + \bar{\beta}_m)\,, \tag{57}$$

where the relationship $\|\zeta\| \leq \frac{V^{1/2}}{\lambda_{min}^{1/2}\{P\}}$ was used. Hence, one can directly obtain the inequality $\dot{V} \leq -\frac{2\epsilon\phi_b}{\lambda_{max}\{P\}}V + \frac{2\|PB\|}{\lambda_{min}^{1/2}\{P\}}V^{1/2}(\kappa_\eta|C_\eta\eta| + \kappa_e|e| + \bar{\beta}_m)$, or, equivalently,

$$\dot{W}_v \leq -\frac{\epsilon\phi_b}{\lambda_{max}\{P\}}W_v + \frac{\|PB\|}{\lambda_{min}^{1/2}\{P\}}(\|C_\eta A_\eta\|\|\eta\| + \kappa_e|e| + \bar{\beta}_m)\,, \tag{58}$$

where $W_v := V^{1/2}$.

Moreover, reminding that $\dot{y} = [-l_0 e + \sigma + \dot{y}_m]$, then from (5) the inverse dynamics is given by $\dot{\eta} = A_\eta \eta + B_\eta[-l_0 e + \sigma + \dot{y}_m]$. Thus, one can put together the e-dynamics ($\dot{e} = -l_0 e + \sigma$) and the inverse dynamics and write

$$\dot{x}_\eta = A_{x\eta} x_\eta + B_\sigma \sigma + B_m \dot{y}_m\,, \quad x_\eta := \left[\,\eta^T \;\; e\,\right]^T\,, \tag{59}$$

where $A_{x\eta} := \begin{bmatrix} A_\eta & -l_0 B_\eta \\ 0 & -l_0 \end{bmatrix}$, $B_\sigma := \left[\,B_\eta^T \;\; 1\,\right]^T$ and $B_m := \left[\,B_\eta^T \;\; 0\,\right]^T$. Then, defining $V_\eta := x_\eta^T P_\eta x_\eta$, with $P_\eta = P_\eta^T > 0$ satisfying $A_{x\eta}^T P_\eta + P_\eta A_{x\eta} = -2I$, since $A_{x\eta}$ is a Hurwitz matrix, then one can obtain

$$\dot{V}_\eta \leq -\frac{2}{\lambda_{max}\{P_\eta\}} V_\eta + 2\|P_\eta B_\sigma\| \frac{V_\eta^{1/2}}{\lambda_{min}^{1/2}\{P_\eta\}} |\sigma| + \\ + 2\|P_\eta B_m\| \frac{V_\eta^{1/2}}{\lambda_{min}^{1/2}\{P_\eta\}} |\dot{y}_m|\,,$$

since $\|x_{x\eta}\| \leq \frac{V_\eta^{1/2}}{\lambda_{min}^{1/2}\{P_\eta\}}$. Equivalently, with $W_\eta := V_\eta^{1/2}$, one has

$$\dot{W}_\eta \leq -\frac{1}{\lambda_{max}\{P_\eta\}} W_\eta + \frac{\|P_\eta B_\sigma\|}{\lambda_{min}^{1/2}\{P_\eta\}} |\sigma| + \frac{\|P_\eta B_m\|}{\lambda_{min}^{1/2}\{P_\eta\}} |\dot{y}_m|\,. \tag{60}$$

Now, reminding that

$$|\hat{\phi}_1| \leq \|\zeta\| \leq \frac{V^{1/2}}{\lambda_{min}^{1/2}\{P\}} = \frac{W_v}{\lambda_{min}^{1/2}\{P\}}\,,$$

and

$$|\hat{\phi}_1(\sigma)| := \left[\frac{\phi_a}{(|\sigma|^{1/2} + \delta)} + \phi_b\right] |\sigma|\,,$$

then $|\hat{\phi}_1(\sigma)| \geq \phi_b |\sigma|$ and $|\sigma| \leq \frac{W_v}{\phi_b \lambda_{min}^{1/2}\{P\}}$. From (58) and (60), one has the following pair of inequalities:

$$\dot{W}_\eta \leq -k_{\eta 1} W_\eta + k_{\eta 2} W_v + k_{\eta 3} |\dot{y}_m|\,, \tag{61}$$

$$\dot{W}_v \leq -k_{v1} W_v + k_{v2} W_\eta + k_{v3} \bar{\beta}_m\,, \tag{62}$$

where $k_{\eta 1} := \frac{1}{\lambda_{max}\{P_\eta\}}$, $k_{\eta 2} := \frac{\|P_\eta B_\sigma\|}{\phi_b \lambda_{min}\{P_\eta\}}$, $k_{\eta 3} := \frac{\|P_\eta B_m\|}{\lambda_{min}^{1/2}\{P_\eta\}}$, $k_{v1} := \frac{\epsilon \phi_b}{\lambda_{max}\{P\}}$, $k_{v2} := \frac{\|PB\|(\kappa_e + \|C_\eta A_\eta\|)}{\lambda_{min}^{1/2}\{P\}\lambda_{min}^{1/2}\{P_\eta\}}$, $k_{v3} := \frac{\|PB\|}{\lambda_{min}^{1/2}\{P\}}$ and we use the fact that $|e|, \|\eta\| \leq \|x_\eta\| \leq W_\eta / \lambda_{min}^{1/2}\{P_\eta\}$. Now, let $\bar{W}_v$ and $\bar{W}_\eta$ be the solutions of the differential equations corresponding to the equalities in (61)–(62), with initial conditions $\bar{W}_v(t_s) = W_v(t_s)$ and $\bar{W}_\eta(t_s) = W_\eta(t_s)$. Thus, by using the Comparison Lemma [39], one has $W_v \leq \bar{W}_v$ and $W_\eta \leq \bar{W}_\eta$, $\forall t \in [t_s, t_M)$.

Now, the proof follows by using the Small-Gain Theorem [49] applied to the pair of differential equations corresponding to the equalities in (61)–(62). From Appendix G, for ϕ_b sufficiently large so that

$$\phi_b^2 \geq \frac{\|P_\eta B_\sigma\| \|PB\| (\kappa_e + \kappa_\eta \|C_\eta\|) \lambda_{max}\{P\} \lambda_{max}\{P_\eta\}}{4\epsilon \lambda_{min}^{1/2}\{P\} \lambda_{min}^{3/2}\{P_\eta\}}$$

one can, subsequently, conclude that: $|z|$ converges exponentially to a residual set of order $\mathcal{O}(1/\phi_b)$, $|\sigma|$ and $|e|$ converges exponentially to a residual set of order $\mathcal{O}(1/\phi_b^2)$ and finite-time escape is avoided in all closed-loop signals. ∎

APPENDIX E AUXILIARY SIGNALS AND NORM BOUNDS

By considering the partitions (30) and (31) of the plant input disturbance $d = d_1(y, \dot{y}, t) + d_2(y, t) + d_3(t)$ and the nominal control $u^n = u_p^n(e) + u_d^n(\sigma) + u_i^n(t) + u_m^n(t)$, one can decompose the disturbance d_σ in (13) as $d_\sigma := \beta_1 + \sigma_a$, leading to $\dot{\sigma} = k_p u + \beta_1 + \sigma_a$, where β_1 is the σ-independent signal

$$\beta_1 := k_p u_d^n(\sigma) + (l_0 - a_p)\sigma + k_p d_1(y, \dot{y}, t)\,, \tag{63}$$

and σ_a is the *auxiliary signal*

$$\sigma_a := (l_0 - a_p)(-l_0 e + \dot{y}_m) + k_p(u_p^n + u_i^n + u_m^n) - \dot{\sigma}_m \\ + k_p(d_2 + d_3) - C_\eta \eta\,. \tag{64}$$

The time derivative of the auxiliary signal σ_a is σ-dependent, but can be decomposed in three signals: (i) β_2, which is σ-dependent; (ii) β_e, which is e-dependent; and β_m, which is an exogenous uniformly norm-bounded time-varying signal.

In fact, $\dot{\sigma}_a$ can be written as $\dot{\sigma}_a := -(l_0 - a_p) l_0 \dot{e} + k_p \frac{du_p^n(e)}{de} \dot{e} + k_p \bar{u}_i^n + k_p \dot{u}_m^n - \ddot{\sigma}_m + (l_0 - a_p)\ddot{y}_m + k_p \dot{d}_2 + k_p \dot{d}_3 - C_\eta \dot{\eta}$. Now, since $\dot{d}_2 = \frac{\partial d_2(y,t)}{\partial y}\dot{y} + \frac{\partial d_2(y,t)}{\partial t}$, $\dot{y} = -l_0 e + \sigma + \dot{y}_m$, $\dot{e} = -l_0 e + \sigma$ and $\dot{\eta} = A_\eta \eta + B_\eta \dot{y}$, one can write

$$\dot{\sigma}_a := \beta_2 + \beta_e + \beta_m\,, \tag{65}$$

where

$$\beta_m := k_p \dot{u}_m^n - \ddot{\sigma}_m + (l_0 - a_p)\ddot{y}_m + k_p \frac{\partial d_2(y,t)}{\partial y} \dot{y}_m \\ + k_p \dot{d}_3 - C_\eta B_\eta \dot{y}_m\,, \tag{66}$$

$$\beta_e := l_0 \left[(l_0 - a_p) l_0 - \frac{du_p^n(e)}{de} + k_p l_0 \frac{\partial d_2(y,t)}{\partial y} \right. \\ \left. + C_\eta B_\eta\right] e - C_\eta A_\eta \eta + k_p \frac{\partial d_2(y,t)}{\partial t}\,, \tag{67}$$

$$\beta_2 := \left[-(l_0 - a_p) l_0 + k_p \frac{du_p^n(e)}{de} + k_p \frac{\partial d_2(y,t)}{\partial y} \right. \\ \left. - C_\eta B_\eta\right] \sigma + k_p \bar{u}_i^n\,. \tag{68}$$

A. AUXILIARY NORM BOUNDS

In this section, the norm bounds for the β-terms are obtained. From Assumption **(A4)**, one can obtain a non-negative constant $\bar{c}_\sigma$, such that $|k_p u_d^n + (l_0 - a_p)\sigma| \leq \bar{c}_\sigma |\sigma|$. Hence, from Assumptions **(A0)–(A1)**, the disturbance β_1 in (63) satisfies $|\beta_1| \leq |k_p u_d^n + (l_0 - a_p)\sigma| + |k_p d_1| \leq [\bar{c}_\sigma + \bar{k}_p(k_{d1}|y| + k_{d2}|\dot{y}| + k_{d3})]|\sigma|$. Moreover, recalling that $y = e + y_m$ and $\dot{e} = -l_0 e + \sigma$, thus $\dot{y} = \dot{e} + \dot{y}_m = -l_0 e + \sigma + \dot{y}_m$ and

$$|\beta_1| \leq (\bar{k}_{d1}|e| + \bar{k}_{d2}|\sigma| + \bar{k}_{d3})|\sigma|\,, \tag{69}$$

with appropriate known constants $\bar{k}_{d1}, \bar{k}_{d2}, \bar{k}_{d3} \geq 0$, since y_m and $\dot{y}_m$ are uniformly norm-bounded signals.

From Assumption **(A3)**, the term $k_p\dot{d}_3(t)$ of the signal β_m defined in (66) satisfies $|k_p\dot{d}_3(t)| \leq k_p\alpha_{d3}(t)$. Thus, β_m is a uniformly norm-bounded signal which satisfies

$$|\beta_m| \leq \bar{k}_p|\dot{u}_m^n| + |\ddot{\sigma}_m| + (l_0 + \bar{a}_p)|\ddot{y}_m| + \bar{k}_p k_{d4}|\dot{y}_m| + \bar{k}_p\alpha_{d3} + \|C_\eta B_\eta\||\dot{y}_m|\,. \tag{70}$$

From Assumptions **(A2)** and **(A4)**, one can subsequently conclude that: (i) the term β_e satisfies

$$|\beta_e| \leq \|C_\eta A_\eta\|\|\eta\| + \kappa_e|e| + \bar{k}_p k_{d5}|y_m| + \bar{k}_p\alpha_{d2}\,, \tag{71}$$

where $\kappa_e := l_0\left[(l_0 + \bar{a}_p)l_0 + c_{e2} + \bar{k}_p l_0 k_{d4} + \|C_\eta B_\eta\|\right] + \bar{k}_p k_{d5}$; and (ii) the term β_2 satisfies

$$|\beta_2| \leq (k_\sigma + c_{i\sigma}|\sigma| + c_{ie}|e|)|\sigma|\,, \tag{72}$$

where $k_\sigma := \left[(l_0 + \bar{a}_p)l_0 + \bar{k}_p c_{e2} + \bar{k}_p k_{d4} + \|C_\eta B_\eta\|\right]$.

NORM BOUNDS ρ_1 AND ρ_2

From (50) and (69), one can write $\phi_b|\sigma||\alpha_1| \leq |\hat{\phi}_1||\alpha_1| = |\beta_1| \leq (\bar{k}_{d1}|e| + \bar{k}_{d2}|\sigma| + \bar{k}_{d3})|\sigma|$, where the lower norm-bound comes from the fact that $\hat{\phi}_1 > \phi_b|\sigma|$, with $\hat{\phi}_1$ defined in (26). Hence, one has $|\alpha_1| < \rho_1$, where

$$\rho_1 := \frac{(\bar{k}_{d1}|e| + \bar{k}_{d2}|\sigma| + \bar{k}_{d3})}{\phi_b}\,.$$

Analogously, from (50) and (72), one can write $\phi_b^2|\sigma||\alpha_2| \leq |\hat{\phi}_1\hat{\phi}_1'||\alpha_2| = |\beta_2| \leq (k_\sigma + c_{i\sigma}|\sigma| + c_{ie}|e|)|\sigma|$, which leads to the norm bound $|\alpha_2| < \rho_2$, where

$$\rho_2 := \frac{(k_\sigma + c_{i\sigma}|\sigma| + c_{ie}|e|)}{\phi_b^2}\,.$$

APPENDIX F GAIN FUNCTIONS DESIGN

The variable gains κ_1 and κ_2 are designed so that the matrix Q, appearing in (54), satisfies $Q - 2\epsilon I > 0$. One possibility is to set

$$\kappa_2 = 2\epsilon\kappa_1 + \gamma\,, \tag{73}$$

which leads to

$$Q - 2\epsilon I = \begin{bmatrix} k_q & 2\epsilon\alpha_1 - \alpha_2 \\ 2\epsilon\alpha_1 - \alpha_2 & 2\epsilon \end{bmatrix},$$

with $k_q := 2(\gamma k_p - 4\epsilon^2)k_p\kappa_1 + 4\epsilon k_p\gamma - 2\gamma k_p\alpha_1 + 4\epsilon\alpha_2 - 2\epsilon$. One has that $Q - 2\epsilon I$ is positive definite for every value of (t, e, σ) if

$$(\gamma k_p - 4\epsilon^2)k_p\kappa_1 > \frac{1}{4\epsilon}(2\epsilon\alpha_1 - \alpha_2)^2 - 2\epsilon\alpha_2 + \gamma k_p(\alpha_1 - 2\epsilon) + \epsilon\,. \tag{74}$$

It is clear that inequality (74) holds if the following one is valid

$$(\gamma k_p - 4\epsilon^2)k_p\kappa_1 \geq \left[\frac{1}{4\epsilon}(2\epsilon\rho_1 + \rho_2)^2 + 2\epsilon\rho_2 + \gamma k_p(\rho_1 + 2\epsilon) + \epsilon\right], \tag{75}$$

with γ satisfying $\gamma k_p - 4\epsilon^2 > 0$, k_p being considered as an uncertain parameter and ρ_1 and ρ_2 being known norm bounds for α_1 and α_2, respectively, obtained in what follows by using the available norm bounds for β_1 and β_2.

IMPLEMENTATION OF THE VARIABLE GAIN κ_1

The gain κ_1 is designed to satisfy (75), which can be rewritten as

$$4\epsilon k_p(\gamma k_p - 4\epsilon^2)\kappa_1 > \left[\rho^2 + 8\epsilon^2\rho_2 + 4\epsilon\gamma k_p\rho_1 + 8\epsilon^2\gamma k_p + 4\epsilon^2\right], \tag{76}$$

where $\rho := 2\epsilon\rho_1 + \rho_2 = \frac{(\bar{k}_{d2}\phi_b + \bar{k}_p c_{i\sigma})}{\phi_b^2}|\sigma| + \frac{(\bar{k}_{d1}\phi_b + \bar{k}_p c_{ie})}{\phi_b^2}|e| + \frac{(\bar{k}_{d3}\phi_b + k_\sigma)}{\phi_b^2}$. In addition, one sufficient condition to assure that (76) holds is given by

$$4\epsilon k_p(\gamma k_p - 4\epsilon^2)\kappa_1 > \left[\rho^2 + (8\epsilon^2 + 2\gamma k_p)\rho + 8\epsilon^2\gamma k_p + 4\epsilon^2\right], \tag{77}$$

by noting that $\rho \geq \rho_2$ and $\rho \geq 2\epsilon\rho_1$. Hence, since ρ, ρ_1 and ρ_2 are linearly related to $|\sigma|$ and $|e|$ and $8\epsilon^2\gamma k_p + 4\epsilon^2$ is a constant, one can select κ_1 as

$$\kappa_1 := (\kappa_a|\sigma| + \kappa_b|e| + \kappa_c)^2 + \kappa_d := \kappa^2 + \kappa_d\,, \tag{78}$$

with $\kappa := (\kappa_a|\sigma| + \kappa_b|e| + \kappa_c)$ and positive constants $\kappa_a, \kappa_b, \kappa_c$ and κ_d designed to assure that (77) holds. One possible design is as follows. Firstly, restrict γ (large enough) to satisfy $4\epsilon k_p(\gamma k_p - 4\epsilon^2) > 1$, and restrict κ_c to satisfy $\kappa_c > \frac{(8\epsilon^2 + 2\gamma k_p)}{[4\epsilon k_p(\gamma k_p - 4\epsilon^2) - 1]}$. Hence, one has that $\kappa > \frac{(8\epsilon^2 + 2\gamma k_p)}{[4\epsilon k_p(\gamma k_p - 4\epsilon^2) - 1]}$ and, consequently, $4\epsilon k_p(\gamma k_p - 4\epsilon^2)\kappa^2 > \kappa^2 + (8\epsilon^2 + 2\gamma k_p)\kappa$. Secondly, restrict κ_d to satisfies

$$\kappa_d > \frac{(8\epsilon^2\gamma k_p + 4\epsilon^2)}{4\epsilon k_p(\gamma k_p - 4\epsilon^2)}\,,$$

one has $4\epsilon k_p(\gamma k_p - 4\epsilon^2)(\kappa^2 + \kappa_d) > \kappa^2 + (8\epsilon^2 + 2\gamma k_p)\kappa + (8\epsilon^2\gamma k_p + 4\epsilon^2)$. Thirdly, restricting κ_a, κ_b and κ_c to satisfy

$$\kappa_a > \frac{(\bar{k}_{d2}\phi_b + \bar{k}_p c_{i\sigma})}{\phi_b^2}\,, \quad \kappa_b > \frac{(\bar{k}_{d1}\phi_b + \bar{k}_p c_{ie})}{\phi_b^2}\,,$$

and $\kappa_c > \frac{(\bar{k}_{d3}\phi_b + k_\sigma)}{\phi_b^2}$, one has that $\kappa = (\kappa_a|\sigma| + \kappa_b|e| + \kappa_c) > \rho$, leading to the conclusion that $\kappa^2 + (8\epsilon^2 + 2\gamma k_p)\kappa > \rho^2 + (8\epsilon^2 + 2\gamma k_p)\rho$ and, consequently, $4\epsilon k_p(\gamma k_p - 4\epsilon^2)(\kappa^2 + \kappa_d) > \rho^2 + (8\epsilon^2 + 2\gamma k_p)\rho + (8\epsilon^2\gamma k_p + 4\epsilon^2)$. Fourthly, restricting κ_c to satisfy

$$\kappa_c > \max\left\{\frac{(8\epsilon^2 + 2\gamma k_p)}{[4\epsilon k_p(\gamma k_p - 4\epsilon^2) - 1]}\,, \frac{(\bar{k}_{d3}\phi_b + k_\sigma)}{\phi_b^2}\right\},$$

one has that (77) holds.

DSSC STATE-DEPENDENT FUNCTIONS

Now, we will provide some additional restrictions to the parameters κ_a, κ_b and ϕ_b, so that the DSSC's state-dependent functions $k_o\tau_{av} > 0$ and $\tau_m > 0$ are well-defined for all finite values of σ, e. Two sufficient conditions for that are

$$\left[\kappa_1'\hat{\phi}_1 + \kappa_1\hat{\phi}_1'\right] > 0\,,$$

and

$$\left[\frac{\partial \kappa_1}{\partial e}[-l_0 e+\sigma]+\frac{\partial \kappa_1}{\partial t}+\kappa_2\hat{\phi}_1'\right]>0\,.$$

From (78), one has $\kappa_1'=\frac{\partial \kappa_1}{\partial \sigma}=2(\kappa_a|\sigma|+\kappa_b|e|+\kappa_c)\kappa_a \text{sgn}(\sigma)$, $\frac{\partial \kappa_1}{\partial e}=2(\kappa_a|\sigma|+\kappa_b|e|+\kappa_c)\kappa_b \text{sgn}(e)$ and $\frac{\partial \kappa_1}{\partial t}=0$. In addition, recall that $\hat{\phi}_1:=\frac{\phi_a\sigma}{(|\sigma|^{1/2}+\delta)}+\phi_b\sigma$ and $\hat{\phi}_1'=\phi_a\left[\frac{(|\sigma|^{1/2}+2\delta)}{2(|\sigma|^{1/2}+\delta)^2}\right]+\phi_b$.

Hence, one can directly conclude that $\kappa_1'\hat{\phi}_1>0$, leading to $\left[\kappa_1'\hat{\phi}_1+\kappa_1\hat{\phi}_1'\right]>0$. Moreover, since $\kappa_2=2\epsilon\kappa_1+\gamma$, one has $\left[\frac{\partial \kappa_1}{\partial e}[-l_0e+\sigma]+\frac{\partial \kappa_1}{\partial t}+\kappa_2\hat{\phi}_1'\right]=\left[\frac{\partial \kappa_1}{\partial e}[-l_0e+\sigma]+(2\epsilon\kappa_1+\gamma)\hat{\phi}_1'\right]>0$, if the following inequality is valid

$$(2\epsilon\kappa_1+\gamma)\hat{\phi}_1'>\left|\frac{\partial \kappa_1}{\partial e}[-l_0e+\sigma]\right|\,. \tag{79}$$

On the other hand,

$$\left|\frac{\partial \kappa_1}{\partial e}[-l_0e+\sigma]\right|\leq 2(\kappa_a|\sigma|+\kappa_b|e|+\kappa_c)\kappa_b(l_0|e|+|\sigma|)\,,$$

and

$$(2\epsilon\kappa_1+\gamma)\hat{\phi}_1'=(2\epsilon[(\kappa_a|\sigma|+\kappa_b|e|+\kappa_c)^2+\kappa_d]+\gamma)\hat{\phi}_1'\,.$$

Now, if $(2\epsilon[(\kappa_a|\sigma|+\kappa_b|e|+\kappa_c)^2+\kappa_d]+\gamma)\hat{\phi}_1'>2(\kappa_a|\sigma|+\kappa_b|e|+\kappa_c)\kappa_b(l_0|e|+|\sigma|)$ then the DSSC's dynamics functions are well-defined. Moreover, note that the following inequality is a sufficient condition

$$\begin{aligned}&2\epsilon(\kappa_a|\sigma|+\kappa_b|e|+\kappa_c)^2\hat{\phi}_1'\\&\quad>2(\kappa_a|\sigma|+\kappa_b|e|+\kappa_c)\kappa_b(l_0|e|+|\sigma|)\,,\end{aligned}$$

or, the following one

$$\epsilon(\kappa_a|\sigma|+\kappa_b|e|+\kappa_c)\phi_b>\kappa_b(l_0|e|+|\sigma|)\,,$$

where we use the fact that

$$\hat{\phi}_1'=\left[\phi_a\left[\frac{(|\sigma|^{1/2}+2\delta)}{2(|\sigma|^{1/2}+\delta)^2}\right]+\phi_b\right]>\phi_b\,.$$

Finally, one can guarantee that the DSSC's dynamics functions are well-defined, by selecting $\phi_b>\frac{l_0}{\epsilon}$ and $\kappa_a>\frac{\kappa_b}{l_0}$. This is summarized in Table 1.

APPENDIX G STABILITY ANALYSIS VIA SMALL-GAIN THEOREM

The equalities in (61)–(62) are given by

$$\dot{\bar{W}}_\eta=-k_{\eta 1}\bar{W}_\eta+k_{\eta 2}W_v+k_{\eta 3}|\dot{y}_m|\,, \tag{80}$$
$$\dot{\bar{W}}_v=-k_{v1}\bar{W}_v+k_{v2}W_\eta+k_{v3}\bar{\beta}_m\,, \tag{81}$$

which can be rewritten as

$$\dot{\mathcal{X}}_1=-\lambda_1\mathcal{X}_1+\frac{g_1}{\phi_b}\mathcal{X}_2+\mathcal{U}_1\,, \tag{82}$$
$$\dot{\mathcal{X}}_2=-\lambda_2\phi_b\mathcal{X}_2+g_2\mathcal{X}_1+\mathcal{U}_2\,, \tag{83}$$

where $\mathcal{X}_1:=\bar{W}_\eta$, $\lambda_1:=\frac{1}{\lambda_{max}\{P_\eta\}}$, $\mathcal{U}_1:=g_1(W_v-\mathcal{X}_2)/\phi_b+\bar{g}_1|\dot{y}_m|$, $g_1=\frac{\|P_\eta B_\sigma\|}{\lambda_{min}\{P_\eta\}}$, $\bar{g}_1=\frac{\|P_\eta B_m\|}{\lambda_{min}^{1/2}\{P_\eta\}}$, $\mathcal{X}_2:=\bar{W}_v$, $\lambda_2:=\frac{\epsilon}{\lambda_{max}\{P\}}$, $\mathcal{U}_2:=g_2(W_\eta-\mathcal{X}_1)+\bar{g}_2\bar{\beta}_m$, $g_2:=\frac{\|PB\|(\kappa_e+\kappa_\eta\|C_\eta\|)}{\lambda_{min}^{1/2}\{P\}\lambda_{min}^{1/2}\{P_\eta\}}$ and $\bar{g}_2:=\frac{\|PB\|}{\lambda_{min}^{1/2}\{P\}}$. Thus, one can write

$$\mathcal{X}_1A\leq e^{-\lambda_1(t-t_s)}\mathcal{X}_1(t_s)+\frac{\gamma_1}{\phi_b}\|\mathcal{X}_2\|_\infty+\frac{1}{\lambda_1}\|\mathcal{U}_1\|_\infty\,, \tag{84}$$
$$\mathcal{X}_2\leq e^{-\lambda_2\phi_b(t-t_s)}\mathcal{X}_2(t_s)+\frac{\gamma_2}{\phi_b}\|\mathcal{X}_1\|_\infty+\frac{1}{\lambda_2\phi_b}\|\mathcal{U}_2\|_\infty\,, \tag{85}$$

where $\gamma_1:=\frac{g_1}{\lambda_1}$ and $\gamma_2:=\frac{g_2}{\lambda_2}$.

Now, one can apply [49, Theorem 2.1] and conclude that the system (82) and (83) with inputs $\mathcal{U}_1$ and $\mathcal{U}_2$, outputs $\mathcal{Y}_1=\mathcal{X}_1$ and $\mathcal{Y}_2=\mathcal{X}_2$ and states $\mathcal{X}_1$ and $\mathcal{X}_2$ is IOpS, satisfying

$$\|\mathcal{X}(t)\|\leq\beta_{\mathcal{X}}(\|\mathcal{X}(t_s)\|,t-t_s)+\alpha_{\mathcal{X}}(\|\mathcal{U}(t)\|_\infty)\,, \tag{86}$$

for some class-$\mathcal{KL}$ function $\beta_{\mathcal{X}}$ and some class-$\mathcal{K}$ function $\alpha_{\mathcal{X}}$, provided that there exist $k_l\geq 0$ and class-$\mathcal{K}_\infty$ functions $\mathcal{F}_1(s)+s$ and $\mathcal{F}_2(s)+s$ such that

$$\mathcal{F}_2(\gamma_2(\mathcal{F}_1(\gamma_1 s)+\gamma_1 s))+\gamma_2(\mathcal{F}_1(\gamma_1 s)+\gamma_1 s)\leq s\,,\quad \forall s\geq s_l\,.$$

In particular, for $\mathcal{F}_1(s)=\mathcal{F}_2(s)=s$ and $k_l=0$, one has the following condition $4\gamma_1\gamma_2\leq\phi_b^2$.

Now, since $W_v<\bar{W}_v=\mathcal{X}_2$, one has $[W_v(t)-\mathcal{X}_2(t)]<0$, $\forall t\in[t_s,t_M)$, from which one can, subsequently, conclude that $\mathcal{U}_1(t):=g_1[W_v(t)-\mathcal{X}_2(t)]+\bar{g}_1|\dot{y}_m(t)|<\bar{g}_1|\dot{y}_m(t)|$, $\forall t\in[t_s,t_M)$ and

$$\|\mathcal{U}_1\|_\infty<\bar{g}_1\|\dot{y}_m\|_\infty\,.$$

Analogously, one has

$$\|\mathcal{U}_2\|_\infty<\bar{g}_2\|\bar{\beta}_m\|_\infty\,,$$

since $W_\eta<\bar{W}_\eta=\mathcal{X}_1$. Thus, $\|\mathcal{U}\|_\infty<\bar{g}_1\|\dot{y}_m\|_\infty+\bar{g}_2\|\bar{\beta}_m\|_\infty$ is uniformly bounded by a ϕ_b-independent constant. Hence, from (86), one has that $\mathcal{X}(t)$, $\mathcal{X}_1(t)$, $\mathcal{X}_2(t)$ converge to a residual set independent of ϕ_b and the initial conditions. Now, backing to (85), one can conclude that $\mathcal{X}_2(t)$ converges to a residual set of order $\mathcal{O}(1/\phi_b)$. Finally, reminding that

$$|\hat{\phi}_1|,|z|\leq\|\zeta\|\leq\frac{V^{1/2}}{\lambda_{min}^{1/2}\{P\}}=\frac{W_v}{\lambda_{min}^{1/2}\{P\}}\leq\frac{\mathcal{X}_2}{\lambda_{min}^{1/2}\{P\}}\,,$$

and $|\hat{\phi}_1|\geq\phi_b|\sigma|$, the one has that $|z|$ converges to a residual set of order $\mathcal{O}(1/\phi_b)$ and $|\sigma|$ (and $|e|$) converges to a residual set of order $\mathcal{O}(1/\phi_b^2)$. ∎

ACRONYMS

DSSC Dynamic Smooth Sliding Control
PID Proportional-Integral-Derivative
SSC Smooth Sliding Control
STA Super-Twisting Algorithm
UAV Unmanned Aerial Vehicle
VGSTA Variable Gain Super-Twisting Algorithm

REFERENCES

[1] D. Peleshko, T. Rak, J. R. Noennig, V. Lytvyn, and V. Vysotska, "Drone monitoring system DROMOS of urban environmental dynamics," in *Proc. ITPM*, 2020, pp. 178–193.

[2] A. Gynnild, "The robot eye witness: Extending visual journalism through drone surveillance," *Digit. Journalism*, vol. 2, no. 3, pp. 334–343, Jul. 2014.

[3] F. Santoso, M. A. Garratt, M. R. Pickering, and M. Asikuzzaman, "3D mapping for visualization of rigid structures: A review and comparative study," *IEEE Sensors J.*, vol. 16, no. 6, pp. 1484–1507, Mar. 2016.

[4] H. D. Nguyen, I. S. Na, S. H. Kim, G. S. Lee, H. J. Yang, and J. H. Choi, "Multiple human tracking in drone image," *Multimedia Tools Appl.*, vol. 78, no. 4, pp. 4563–4577, Feb. 2019.

[5] S. Kim, G. Anagnostopoulos, E. Barmpounakis, and N. Geroliminis, "Visual extensions and anomaly detection in the pNEUMA experiment with a swarm of drones," *Transp. Res. C, Emerg. Technol.*, vol. 147, Feb. 2023, Art. no. 103966.

[6] E. Barmpounakis and N. Geroliminis, "On the new era of urban traffic monitoring with massive drone data: The pNEUMA large-scale field experiment," *Transp. Res. C, Emerg. Technol.*, vol. 111, pp. 50–71, Feb. 2020.

[7] S. Abdelhay and A. Zakriti, "Modeling of a quadcopter trajectory tracking system using PID controller," *Proc. Manuf.*, vol. 32, pp. 564–571, Jan. 2019.

[8] V. Riviere, A. Manecy, and S. Viollet, "Agile robotic fliers: A morphing-based approach," *Soft Robot.*, vol. 5, no. 5, pp. 541–553, Oct. 2018.

[9] P. E. I. Pounds, D. R. Bersak, and A. M. Dollar, "Stability of small-scale UAV helicopters and quadrotors with added payload mass under PID control," *Auto. Robots*, vol. 33, nos. 1–2, pp. 129–142, Aug. 2012.

[10] C. Bao, Y. Guo, L. Luo, and G. Su, "Design of a fixed-wing UAV controller based on adaptive backstepping sliding mode control method," *IEEE Access*, vol. 9, pp. 157825–157841, 2021.

[11] J. V. Shirabayashi and L. B. Ruiz, "Toward UAV path planning problem optimization considering the Internet of Drones," *IEEE Access*, vol. 11, pp. 136825–136854, 2023.

[12] T. K. Priyambodo, O. A. Dhewa, and T. Susanto, "Model of linear quadratic regulator (LQR) control system in waypoint flight mission of flying wing UAV," *J. Telecommun., Electron. Comput. Eng.*, vol. 12, no. 4, pp. 43–49, 2020.

[13] M. Farrell, J. Jackson, J. Nielsen, C. Bidstrup, and T. McLain, "Error-state LQR control of a multirotor UAV," in *Proc. Int. Conf. Unmanned Aircr. Syst. (ICUAS)*, Jun. 2019, pp. 704–711.

[14] A. Ermeydan and A. Kaba, "Feedback linearization control of a quadrotor," in *Proc. 5th Int. Symp. Multidisciplinary Stud. Innov. Technol. (ISMSIT)*, Oct. 2021, pp. 287–290.

[15] A. Ghassan and H. Zeaid, "Design of an automatic landing system for a UAV using feedback linearization method," in *Proc. ASME Early Career Tech. Conf.*, Fayetteville, AR, USA, 2011, pp. 1–7.

[16] J. A. Moreno and M. Osorio, "A Lyapunov approach to second-order sliding mode controllers and observers," in *Proc. 47th IEEE Conf. Decis. Control*, Dec. 2008, pp. 2856–2861.

[17] J. Mendoza-Avila, J. A. Moreno, and L. M. Fridman, "Continuous twisting algorithm for third-order systems," *IEEE Trans. Autom. Control*, vol. 65, no. 7, pp. 2814–2825, Jul. 2020.

[18] J. A. Moreno, "A linear framework for the robust stability analysis of a generalized super-twisting algorithm," in *Proc. 6th Int. Conf. Electr. Eng., Comput. Sci. Autom. Control (CCE)*, Jan. 2009, pp. 1–6.

[19] A. Davila, J. A. Moreno, and L. Fridman, "Variable gains super-twisting algorithm: A Lyapunov based design," in *Proc. Amer. Control Conf.*, Jun. 2010, pp. 968–973.

[20] Y. B. Shtessel, J. A. Moreno, F. Plestan, L. M. Fridman, and A. S. Poznyak, "Super-twisting adaptive sliding mode control: A Lyapunov design," in *Proc. 49th IEEE Conf. Decis. Control (CDC)*, Dec. 2010, pp. 5109–5113.

[21] I. Castillo, L. Fridman, and J. A. Moreno, "Super-twisting algorithm for systems with uncertain control gain: A Lyapunov based approach," in *Proc. 14th Int. Workshop Variable Struct. Syst. (VSS)*, Jun. 2016, pp. 340–344.

[22] J. A. Moreno and M. Osorio, "Strict Lyapunov functions for the super-twisting algorithm," *IEEE Trans. Autom. Control*, vol. 57, no. 4, pp. 1035–1040, Apr. 2012.

[23] T. Gonzalez, J. A. Moreno, and L. Fridman, "Variable gain super-twisting sliding mode control," *IEEE Trans. Autom. Control*, vol. 57, no. 8, pp. 2100–2105, Aug. 2012.

[24] H. Haimovich, L. Fridman, and J. A. Moreno, "Generalized super-twisting for control under Time- and state-dependent perturbations: Breaking the algebraic loop," *IEEE Trans. Autom. Control*, vol. 67, no. 10, pp. 5646–5652, Oct. 2022.

[25] J. O. Ventura, D. B. Morales, J. P. O. Oliver, and E. S. E. Quesada, "Dynamic sliding mode control with PID surface for trajectory tracking of a multirotor aircraft," *IEEE Access*, vol. 11, pp. 99878–99888, 2023.

[26] I. González-Hernández, S. Salazar, R. Lozano, and O. Ramírez-Ayala, "Real-time improvement of a trajectory-tracking control based on super-twisting algorithm for a quadrotor aircraft," *Drones*, vol. 6, no. 2, p. 36, Jan. 2022.

[27] J. A. C. González, O. Salas-Peña, and J. De León-Morales, "Observer-based super twisting design: A comparative study on quadrotor altitude control," *ISA Trans.*, vol. 109, pp. 307–314, Mar. 2021.

[28] V. K. Tripathi, A. K. Kamath, L. Behera, N. K. Verma, and S. Nahavandi, "Finite-time super twisting sliding mode controller based on higher-order sliding mode observer for real-time trajectory tracking of a quadrotor," *IET Control Theory Appl.*, vol. 14, no. 16, pp. 2359–2371, Nov. 2020.

[29] H. A. B. Anuar, F. Plestan, A. Chriette, and O. Kermorgant, "Super-twisting sliding mode control with adaptive gain of quadrotor with rigid manipulator," in *Proc. 16th Int. Workshop Variable Struct. Syst. (VSS)*, Sep. 2022, pp. 53–58.

[30] S. H. Derrouaoui, Y. Bouzid, and M. Guiatni, "Nonlinear robust control of a new reconfigurable unmanned aerial vehicle," *Robotics*, vol. 10, no. 2, p. 76, May 2021.

[31] N.-S. Kim and T.-Y. Kuc, "Sliding mode backstepping control for variable mass hexa-rotor UAV," in *Proc. 20th Int. Conf. Control*, Oct. 2020, pp. 873–878.

[32] A. J. Peixoto, D. Pereira-Dias, and R. H. R. Andrade, "Smooth robust control applied to quadrotor landing," in *Proc. IEEE 58th Conf. Decis. Control (CDC)*, Dec. 2019, pp. 7875–7880.

[33] L. Hsu, "Smooth sliding control of uncertain systems based on a prediction error," *Int. J. Robust Nonlinear Control*, vol. 7, no. 4, pp. 353–372, Apr. 1997.

[34] L. Hsu, F. Lizarralde, and A. D. De Araujo, "New results on output-feedback variable structure model-reference adaptive control: Design and stability analysis," *IEEE Trans. Autom. Control*, vol. 42, no. 3, pp. 386–393, Mar. 1997.

[35] L. Hsu and R. R. Costa, "Variable structure model reference adaptive control using only input and output measurements—Part I," *Int. J. Control*, vol. 49, no. 2, pp. 399–416, 1989.

[36] T. R. Oliveira, L. Hsu, and E. V. L. Nunes, "Smooth sliding control to overcome chattering arising in classical SMC and super-twisting algorithm in the presence of unmodeled dynamics," *J. Franklin Inst.*, vol. 359, no. 2, pp. 1235–1256, Jan. 2022.

[37] W. G. Serrantola, F. Lizarralde, and A. J. Peixoto, "From the modified smooth sliding control to the super-twisting algorithm: UAV trajectory tracking experimental results," in *Proc. 16th Int. Workshop Variable Struct. Syst. (VSS)*, Sep. 2022, pp. 47–52.

[38] T. Lee, M. Leok, and N. H. McClamroch, "Control of complex maneuvers for a quadrotor UAV using geometric methods on SE(3)," 2010, *arXiv:1003.2005*.

[39] H. K. Khalil, *Nonlinear Systems*, 3rd ed. Upper Saddle River, NJ, USA: Prentice-Hall, 2002.

[40] A. Levant, "Higher-order sliding modes, differentiation and output-feedback control," *Int. J. Control*, vol. 76, nos. 9–10, pp. 924–941, Jan. 2003.

[41] T. R. Oliveira, A. J. Peixoto, and L. Hsu, "Output-feedback exact tracking of uncertain nonlinear systems via dwell-time and norm observers," *Int. J. Robust Nonlinear Control*, vol. 23, pp. 483–513, Mar. 2013.

[42] T. R. Oliveira, A. J. Peixoto, E. V. L. Nunes, and L. Hsu, "Output-feedback exact tracking of uncertain nonlinear systems via dwell-time and norm observers," *Int. J. Adapt. Control Signal Process.*, vol. 21, pp. 692–707, May 2007.

[43] A. J. Peixoto, F. Lizarralde, and L. Hsu, "Further results on smooth sliding control of uncertain systems," in *Proc. Amer. Control Conf.*, vol. 3, Jun. 2002, pp. 2380–2385.

[44] A. J. Peixoto, F. Lizarralde, and L. Hsu, "Experimental results on smooth sliding control of uncertain systems," in *Proc. 40th IEEE Conf. Decis. Control*, vol. 1, Dec. 2001, pp. 928–933.

[45] L. Derafa, A. Benallegue, and L. Fridman, "Super twisting control algorithm for the attitude tracking of a four rotors UAV," *J. Franklin Inst.*, vol. 349, no. 2, pp. 685–699, Mar. 2012.
[46] V. I. Utkin, "Scope of the theory of sliding modes," in *Sliding Modes in Control and Optimization*. Berlin, Germany: Springer-Verlag, 1992, pp. 1–11.
[47] H. Chen, H. Bai, and C. N. Taylor, "Invariant-EKF design for quadcopter wind estimation," in *Proc. Amer. Control Conf. (ACC)*, Jun. 2022, pp. 1236–1241.
[48] C. Edwards and S. Spurgeon, *Sliding Mode Control: Theory and Applications*. Boca Raton, FL, USA: CRC Press, 1998.
[49] Z.-P. Jiang, A. R. Teel, and L. Praly, "Small-gain theorem for ISS systems and applications," *Math. Control, Signals, Syst.*, vol. 7, no. 2, pp. 95–120, Jun. 1994.

ALESSANDRO JACOUD PEIXOTO (Member, IEEE) received the degree in electronics engineering from the Federal University of Rio de Janeiro (UFRJ), in 2000, and the M.Sc. and Ph.D. degrees in electrical engineering from COPPE/Federal University of Rio de Janeiro, Brazil, in 2002 and 2007, respectively. In 2011, he joined the Graduate School and Research in Engineering (COPPE), Federal University of Rio de Janeiro. Since 2007, he has been with Brazilian Antartic Program, developing an ROV for underwater inspection, and visited Brazilian Station, Antartic, in November 2007. Currently, he is an Associate Professor with the Department of Electronics and Computer Engineering (DEL/Poli/UFRJ), Federal University of Rio de Janeiro. His research interests include nonlinear control theory, control of uncertain nonlinear systems, sliding mode control, extremum-seeking control, real-time control systems, industrial processes, automation, robotics, and sources of renewable energy. He is a member of Sociedade Brasileira de Automática and the IEEE Control Systems Society. In 2017 and 2020, he received the Award "Prêmio ANP de Inovação Tecnológica" granted by the Brazilian National Agency for Petroleum, Natural Gas and Biofuels (ANP), developing a robot for topside inspection and autonomous drones for oil spill detection in the sea, respectively.

WENDERSON G. SERRANTOLA was born in Ribeirão Preto, Brazil. He received the degree in control and automation engineering from the Federal University of Ouro Preto (UFOP), in 2015, and the M.Sc. degree in electrical engineering from the University of São Paulo (USP), in 2018. He is currently pursuing the Ph.D. degree in electrical engineering with the Federal University of Rio de Janeiro (COPPE/UFRJ). His background includes theoretical and applied research in the mining field and the oil and gas industry, with terrestrial and aerial robots.

FERNANDO LIZARRALDE (Senior Member, IEEE) was born in Bell Ville, Argentina. He received the Ingeniero Electricista degree from Universidad Nacional del Sur, Bahia Blanca, Argentina, in 1989, and the M.Sc. and Ph.D. degrees in electrical engineering from the Federal University of Rio de Janeiro, Rio de Janeiro, Brazil, in 1992 and 1998, respectively. Since 1996, he has been with the Department of Electrical Engineering, Federal University of Rio de Janeiro, where he is currently a Full Professor. From 2010 to 2011, he was a Visiting Researcher with the Center for Automation Technologies and Systems, Rensselaer Polytechnic Institute. His current research interests include nonlinear control systems, adaptive control, variable structure control, visual servoing, stability of nonlinear systems, and their applications to industrial process control, including thermal systems, industrial and cooperative robotics, additive manufacturing, and field and underwater robotics. He is a member of Sociedade Brasileira de Automática and the IEEE Control Systems Society. He was an Associate Editor of the IEEE Control Systems Society Conference Editorial Board, from 2008 to 2015, and IEEE Robotics and Automation Letters from 2015 to 2018.